# Multifunctional hydrogel based on polyvinyl alcohol/chitosan/metal polyphenols for facilitating acute and infected wound healing

Ruigang Zhou [a,1], Junjie Huang [a,1], Wenhai Zhang [a], Weimei Wang [a], Weilong Peng [a], Jun Chen [a], Chenglong Yu [a], Ruonan Bo [a,b], Mingjiang Liu [a,b], Jingui Li [a,b,*]

[a] School of Veterinary Medicine, Jiangsu Co-innovation Center for Prevention and Control of Important Animal Infectious Diseases and Zoonoses, Yangzhou University, Yangzhou, 225009, PR China
[b] Joint International Research Laboratory of Agriculture and Agri-Product Safety, The Ministry of Education of China, Yangzhou University, Yangzhou, Jiangsu, 225009, PR China

## ARTICLE INFO

## ABSTRACT

Bacterial-infected wounds could cause delayed wound healing due to increased inflammation, especially wounds infected by drug-resistant bacteria remain a major clinical problem. However, traditional treatment strategies were gradually losing efficacy, such as the abuse of antibiotics leading to enhanced bacterial resistance. Therefore, there was an urgent need to develop an antibiotic-free multifunctional dressing for bacterially infected wound healing. This study demonstrated the preparation of a multifunctional injectable hydrogel and evaluated its efficacy in treating acute and infected wounds. The hydrogel was prepared by a one-step mixing method, and cross-linked by natural deep eutectic solvent (DES), polyvinyl alcohol (PVA), chitosan (CS), tannic acid (TA), and $Cu^{2+}$ through non-covalent interactions (hydrogen bonds and metal coordination bonds). PVA/CS/DES/CuTA$_{500}$ hydrogel has multiple functional properties, including injectability, tissue adhesion, biocompatibility, hemostasis, broad-spectrum antibacterial, anti-inflammatory, and angiogenesis. Most importantly, in the *MRSA*-infected skin wound model, PVA/CS/DES/CuTA$_{500}$ hydrogel could ultimately accelerate infected wound healing by killing bacteria, activating M2 polarization, inhibiting inflammation, and promoting angiogenesis. In summary, the PVA/CS/DES/CuTA$_{500}$ hydrogel showed great potential as a wound dressing for bacterial infected wounds treatment in the clinic.

## 1. Introduction

Bacterial wound infections associated with skin injuries, burns, and diseases are a major public health challenge facing clinicians due to their huge economic burden and high mortality rate [1–3]. In particular, bacterial infections caused by methicillin-resistant *Staphylococcus aureus* usually cause chronic inflammation, severely inhibit wound proliferation and remodelling, and even seriously lead to sepsis and multiple organ failure [4,5]. Antibiotics are commonly used to kill bacteria quickly, however, antibiotics have many disadvantages such as low bioavailability, large side effects, and easy bacterial resistance [6]. Therefore, it is urgent to develop an antibiotic-free multifunctional dressing for bacterial-infected wound healing and accelerated wound healing/tissue regeneration.

It is well known that wound dressings are indispensable consumables in practical clinical applications [7,8]. However, the design of wound dressings requires careful consideration of many factors, for example, the selection of environmentally friendly raw materials and synthesis methods should be considered. The higher the environmental friendliness, the smaller the burden of discarded wound dressings on the environment, and the better the biocompatibility with the body. Therefore, constructing multifunctional wound dressings, especially new environmentally friendly ones, is particularly urgent. Hydrogel dressings have become a research hotspot due to their excellent swelling, absorption of tissue exudates, maintenance of wound moist environment, and antibacterial and anti-inflammatory properties [9, 10]. Polyvinyl alcohol (PVA) is widely used in biomaterials, biomedicine, and other fields because of its many advantages such as good biocompatibility, high mechanical strength, non-toxicity, and biodegradability [11,12]. Chitosan (CS) is the only naturally occurring

---

cationic polysaccharide with multiple biological activities, including antibacterial properties, biodegradability, excellent adhesion, and good biocompatibility, and has great application prospects in biomedical dressings [13,14]. In addition, hydrogel dressings based on PVA and CS are usually constructed by freeze-thaw cycles, chemical cross-linking, etc [15,16]. CS has a unique crosslinking ability to form hydrogen bonds with PVA due to its amine and hydroxyl groups [17]. However, the safety of the produced hydrogels in applications requiring biocompatibility is severely limited by toxicity issues such as the large residual amount of some substances used to cross-link hydrogels. Therefore, it is necessary to seek certain methods to avoid the adverse effects of covalent crosslinkers.

Deep eutectic solvents (DES) are a new type of green solvent with strong solubility, easy synthesis, better biocompatibility, and sustainable utilization [18,19]. Due to hydrogen bond acceptors (HBA) and hydrogen bond donors (HBD), DES is more likely to interact with polymer structures rich in amino and hydroxyl groups. Therefore, DES has been gradually applied to construct chitosan film dressings [20,21]. Tannic acid (TA) is a polyphenol component widely distributed in plants and marine organisms. It has excellent biological activity and has attracted widespread attention in biomedical fields such as wound dressings [22,23]. TA contains many phenolic and carbonyl groups and can be easily cross-linked with various polymers by forming ionic bonds, hydrogen bonds, and hydrophobic interactions [24,25]. TA can also form metal-polyphenol networks (MPNs) by coordinating with metal ions. Among the numerous metal ions, $Cu^{2+}$ was selected to coordinate with TA to form a copper tannic acid (CuTA) metal-polyphenol network, which imparts antibacterial and anti-inflammatory abilities, promotes wound angiogenesis, and is more conducive to accelerating wound healing [6,26]. By coordinating the interaction between the catechol groups of TA and $Cu^{2+}$, a double-crosslinked hydrogel can be constructed, improving the mechanical strength and stiffness of the hydrogel [27,28]. In addition, it has been found that the dynamic redox catalytic system formed by the polyphenol structure and metal ions can accelerate the gelation of hydrogels at room temperature [29,30], which is conducive to seeking a simple, large-scale, economical, and environmentally friendly method for preparing hydrogels.

Based on this background, we designed and characterized a supramolecular multifunctional hydrogel (PVA/CS/DES/CuTA) cross-linked by natural DES, PVA, CS, TA, and $Cu^{2+}$ through non-covalent interactions (hydrogen bonds and metal coordination). The performance of the hydrogel dressing was characterized and tested, and the potential of the prepared hydrogel dressing as a wound medical dressing was evaluated. In addition, *in vitro* and *in vivo* experiments were conducted to assess the efficacy and mechanism of hydrogel in wound healing, aiming to provide a certain reference for the design and preparation of medical wound dressings (Scheme 1).

## 2. Results and discussion

### 2.1. Preparation and characterization of CuTA and prepared hydrogels

$Cu^{2+}$ and TA containing polyphenol groups self-assembled to generate CuTA through oxidative coupling. Under weak alkalinity and high concentration of $Cu^{2+}$, TA undergoes accelerated self-oxidation to form semiquinone (T′) and quinone (T″), which further chelated with $Cu^{2+}$ to form CuTA with a metal polyphenol network [31–33]. The morphological features of CuTA were first characterized by transmission electron microscopy (TEM, HT7800, Hitachi, Japan) and observed using a scanning electron microscope (SEM, Gemini 300, ZEISS, Germany) equipped with an energy-scattering spectrometer (Oxford X-max20). TEM images showed that the length of CuTA was about 100 nm and the width was about 50 nm (Fig. 1A). Also, the Z-Average (d. nm) of CuTA was about 122 nm, confirming the results (Fig. S1). The Zeta Potential of CuTA was about $-10.1 \pm 1.139$ mV (Fig. S2). In addition, TEM and SEM images showed that CuTA exhibited a uniform nanosheet structure, and

elemental mapping also confirmed that Cu, P, C, O, and S were uniformly distributed in CuTA, with the Cu mass fraction approaching 50 % (Fig. 1B and C). Choline chloride and ethylene glycol prepared DES as hydrogen bond acceptors (HBA) and hydrogen bond donors (HBD). The abbreviations and compositions of the prepared hydrogels in this study were provided in Table S1 in the supporting information. The construction and preparation mechanism of PVA/CS/DES/CuTA hydrogel were briefly described in Scheme 1. PVA/CS/DES/CuTA hydrogel was a physically cross-linked hydrogel constructed by a one-pot mixing method (Video S1). In the preparation process of PVA/CS/DES/CuTA hydrogel, the first step was hydrogen bond crosslinking, including between the phenolic hydroxyl groups in TA and the alcoholic hydroxyl groups in PVA chains and between TA and the amine and hydroxyl groups in CS chains [34,35]. In addition, when the content of CuTA was 500 and 1000 $\mu$g mL$^{-1}$, the secondary crosslinking of PVA/CS/DES/CuTA hydrogel was prepared through the coordination interaction between $Cu^{2+}$ and the phenolic hydroxyl groups in TA, thus successfully constructing the double crosslinked hydrogel [33]. The physicochemical properties of the hydrogel were then measured, and the effect of the hydrogel on the healing of acute and *MRSA*-infected wounds in mice was evaluated.

The internal morphology of freeze-dried samples of PVA/CS, PVA/CS/DES, PVA/CS/DES/CuTA$_{250}$, PVA/CS/DES/CuTA$_{500}$, and PVA/CS/DES/CuTA$_{1000}$ was observed by scanning electron microscopy (SEM). As shown in Fig. 1D, there were no obvious interconnected pores inside PVA/CS and PVA/CS/DES. The internal pores of PVA/CS/DES/CuTA$_{250}$ were slightly larger and irregular, and the pore size distribution was uneven. The pores of PVA/CS/DES/CuTA$_{500}$ and PVA/CS/DES/CuTA$_{1000}$ were denser, presenting a porous honeycomb structure, and the pore arrangement was more uniform and regular. This might be due to the sufficient catechol groups in TA cross-linking through hydrogen bonds and copper ions providing metal coordination bonds, thereby promoting the formation and stability of the hydrogel framework [31, 36]. In addition, EDS was used to analyze the element distribution of PVA/CS/DES/CuTA$_{500}$ hydrogel, and element mapping showed that elements such as C, N, O, and Cu were evenly distributed in the hydrogel (Fig. 1E). FTIR further characterized the chemical structure of the prepared hydrogels. As shown in Fig. 1F and G, the broad peak near 3290 cm$^{-1}$, the peak near 2937 cm$^{-1}$, and 1082 cm$^{-1}$ in the FTIR spectrum were attributed to the stretching vibrations of O-H, C-H, and C-O, respectively, which were characteristic vibration peaks of PVA [37]. In particular, the broad peak around 3290 cm$^{-1}$ became broader in PVA/CS/DES, PVA/CS/DES/CuTA$_{250}$, PVA/CS/DES/CuTA$_{500}$, and PVA/CS/DES/CuTA$_{1000}$ compared with that of PVA due to the enhanced hydrogen bonding between choline chloride and ethylene glycol molecules in DES [38]. The characteristic peaks around 1150 and 1065 cm$^{-1}$ correspond to the bending vibration of the C-O-C bond and the stretching vibration of the C-O bond in CS, respectively. The peaks near 1567 and 1642 cm$^{-1}$ correspond to the stretching vibrations of N-H and C-O, respectively, mainly due to the typical C2 symmetry of chitosan's type 2 crystal structure [39]. In addition, Fig. S3 showed that no new absorption peaks were observed during the synthesis of PVA/CS/DES/CuTA$_{500}$, indicating that the synthesis is an irreversible physical process and no new chemical bonds are formed. Overall, the above results showed that the hydrogels were successfully prepared. Furthermore, the structural characteristics of the prepared hydrogels were characterized using UV–vis spectroscopy. As shown in Figs. S4 and S5, the UV–vis spectrum of CuTA showed the presence of characteristic peaks of TA similar to those reported previously [40]. In addition, compared with CuTA, the peaks of PVA/CS/DES/CuTA$_{250}$, PVA/CS/DES/CuTA$_{500}$, and PVA/CS/DES/CuTA$_{1000}$ hydrogels all showed a small red shift from 310 nm to 320 nm. Importantly, a new broad peak was detected at around 650 nm for the prepared hydrogels, which was attributed to the charge transfer band generated by the coordination between TA and copper ions, demonstrating that the metal coordination of copper ions with phenolic hydroxyl groups led to the formation of
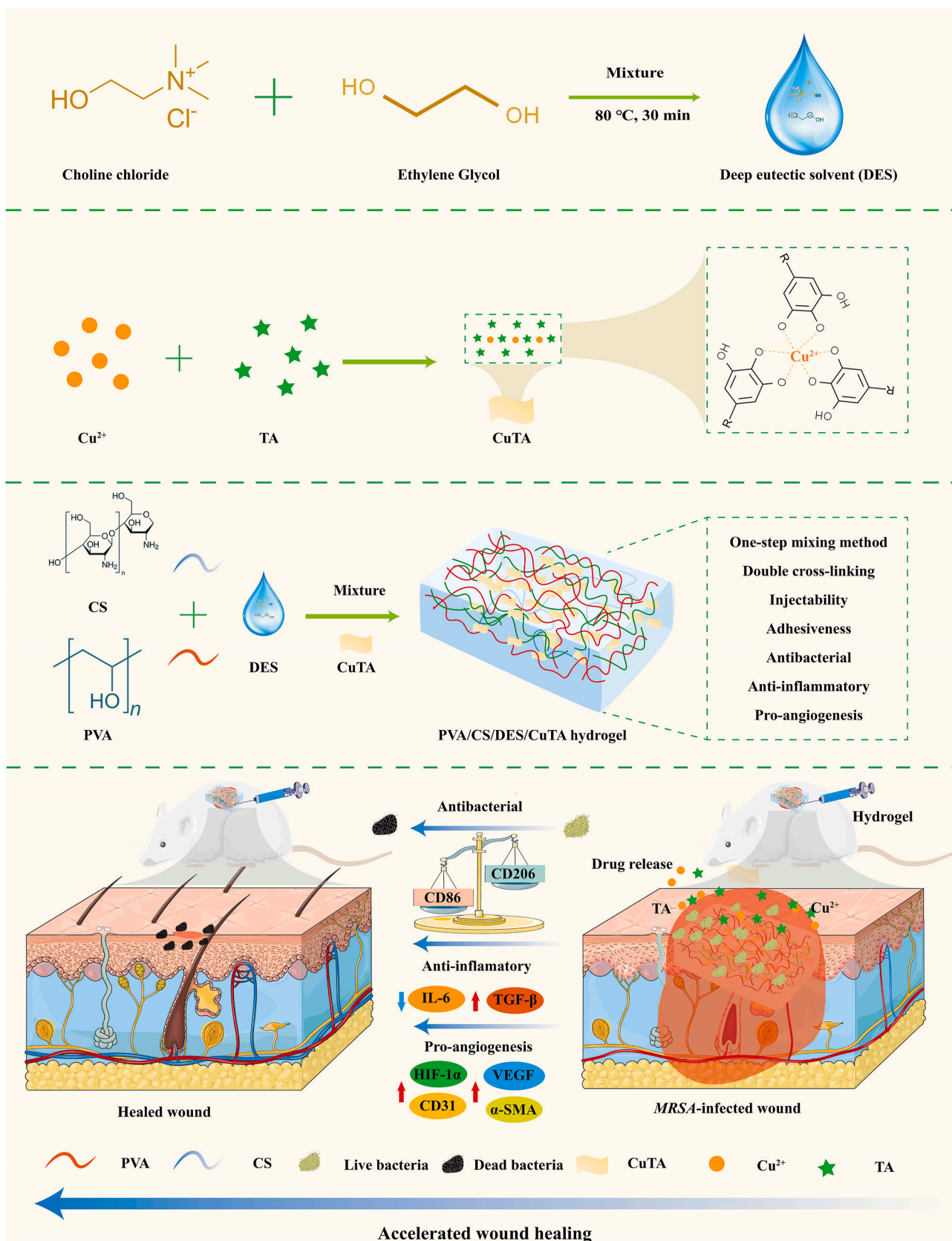
**Scheme 1.** Schematic diagram of PVA/CS/DES/CuTA hydrogel preparation and its application in acute and *MRSA*-infected wound healing.
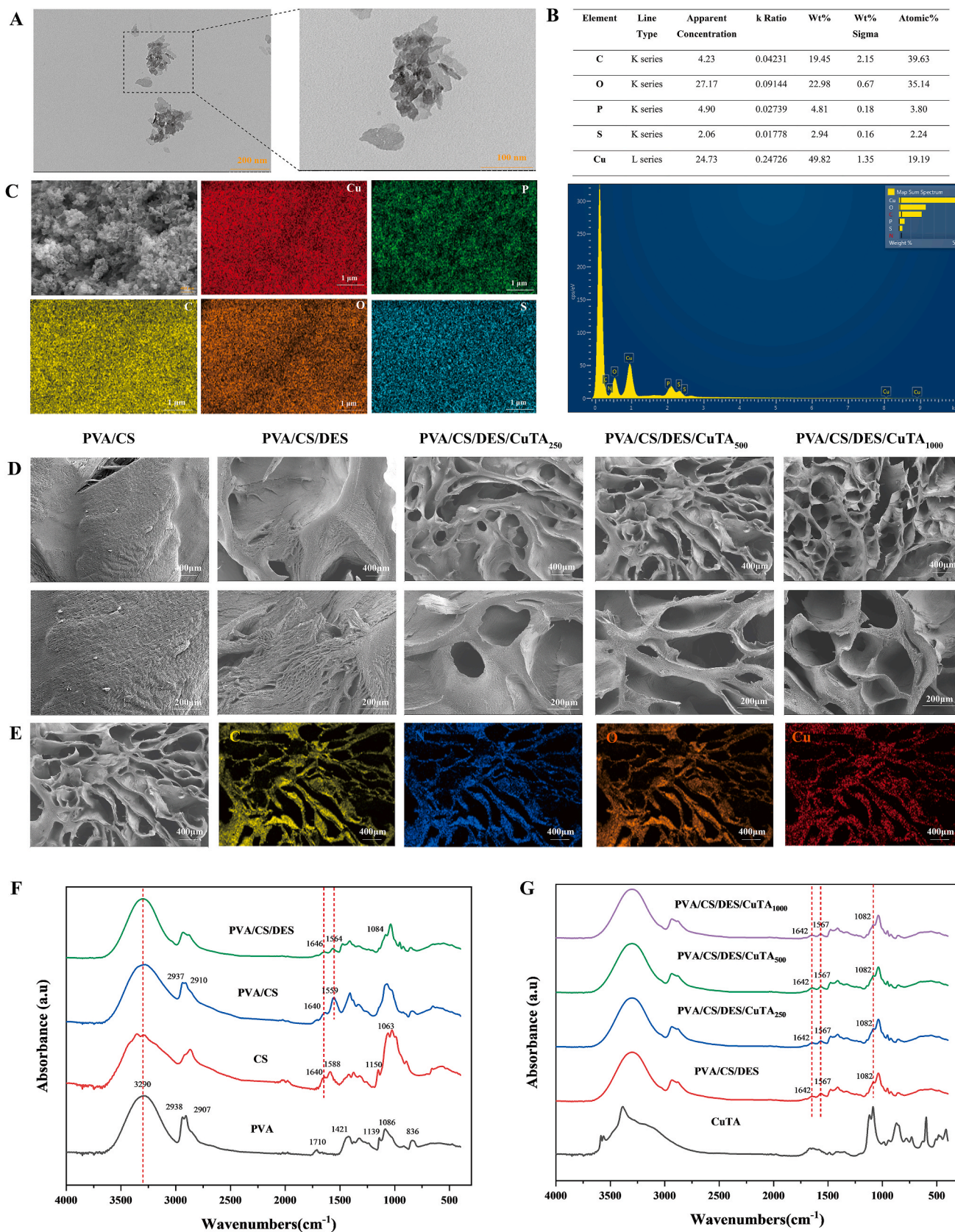
**B**

| Element | Line Type | Apparent Concentration | k Ratio | Wt% | Wt% Sigma | Atomic% |
|---------|-----------|------------------------|---------|------|-----------|---------|
| C | K series | 4.23 | 0.04231 | 19.45 | 2.15 | 39.63 |
| O | K series | 27.17 | 0.09144 | 22.98 | 0.67 | 35.14 |
| P | K series | 4.90 | 0.02739 | 4.81 | 0.18 | 3.80 |
| S | K series | 2.06 | 0.01778 | 2.94 | 0.16 | 2.24 |
| Cu | L series | 24.73 | 0.24726 | 49.82 | 1.35 | 19.19 |

**Fig. 1.** Characterization of CuTA nanoparticles and prepared hydrogels. (**A**) TEM image of CuTA nanoparticles. (**B** and **C**) SEM image and EDS elemental mapping of CuTA nanoparticles (carbon, oxygen, phosphorus, sulfur, and copper). (**D** and **E**) SEM image and EDS elemental mapping (carbon, nitrogen, oxygen, and copper) of prepared hydrogels. (**F** and **G**) FTIR spectra of different freeze-dried hydrogels and their components.

double network hydrogels.

## 2.2. Self-healing, adhesion, and injectability of prepared hydrogels

Hydrogels with excellent physical properties are indispensable for clinical applications. For example, hydrogel dressings with good injectability, adhesiveness, and self-healing properties have excellent adaptability to irregular wounds and help improve drug absorption [41, 42]. As shown in Fig. 2A, the hydrogel precursor solution flowing in the centrifuge tube was transformed into a gel state after adding a specific concentration (500, 1000 µg mL$^{-1}$) of CuTA, demonstrating the formation of dynamic hydrogels on a macroscopic scale. The PVA/CS/-DES/CuTA$_{500}$ could adapt to different shapes, which showed its shape adaptability (Fig. 2B). Hydrogels used to treat skin wounds should also have appropriate adhesion properties to prevent secondary infection [43]. As shown in Fig. 2C, PVA/CS/DES/CuTA$_{500}$ hydrogel could adhere firmly to fresh pig skin regardless of the bending angle of the pig skin. Also, PVA/CS/DES/CuTA$_{500}$ hydrogel exhibited excellent adhesion to biological tissues such as the heart, liver, spleen, and kidney (Fig. 2D). PVA/CS/DES/CuTA$_{500}$ hydrogel could also adhere to non-biological materials such as plastic, glass, iron, and paper (Fig. 2F). The excellent adhesion properties might be attributed to the polyphenol groups, hydrogen bonds, and metal coordination bonds in the prepared hydrogels, which could form non-covalent bonds with amino, hydroxyl, and thiol groups in tissues [44]. Excellent self-healing properties could prevent the hydrogel from rupturing under external stress. Therefore, the self-healing properties of PVA/CS/DES/CuTA$_{500}$ hydrogel were tested. The prepared hydrogel cut into several parts could recover to its original state before cutting within 20 min (Fig. 2E), reflecting the excellent self-healing properties of PVA/CS/DES/CuTA$_{500}$ hydrogel. These results indicated the prepared hydrogel possessed good injectability, self-healing properties, and adhesion, providing multifunctional properties for clinical wound applications.

## 2.3. Rheological properties of prepared hydrogels

Hydrogels are generally soft and wet but have poor mechanical properties, seriously hindering their application in clinical wound dressings [21]. Therefore, the ideal hydrogel should be a solid with a viscoelastic mechanical form [45]. The rheological behavior of PVA/CS/DES/CuTA$_{500}$, and PVA/CS/DES/CuTA$_{1000}$ hydrogels at 25 °C and 37 °C was evaluated using time sweep analysis, representing the mechanical properties of the hydrogels. The time scan analysis results of the prepared hydrogels showed that the storage modulus (G′) at 25 °C (Fig. 2G) and 37 °C (Fig. 2H) was always greater than the loss modulus (G″). In addition, the frequency scan analysis results of the prepared hydrogels also showed a similar trend. The above results showed that the prepared hydrogels behaved as stable viscoelastic solids. To further study the elastic behaviour of the prepared hydrogels, strain sweep tests were performed at a fixed frequency of 1 Hz at 37 °C. The strain sweep results of PVA/CS/DES/CuTA$_{500}$, and PVA/CS/DES/CuTA$_{1000}$ hydrogels were shown in Fig. 2I, it was found that G′ and G″ did not change significantly under 0.1%–100 % strain, and the prepared hydrogels showed G' > G''. Interestingly, all hydrogels did not undergo critical deformation when the strain reached 100 %, and the storage modulus (G′) of all hydrogels was higher than the loss modulus (G″), indicating that the prepared hydrogels were always in a gel state. The possible reason was that PVA, CS, and DES formed strong hydrogen bonds and coordination bonds with copper ions, therefore strongly cross-linking the hydrogel, and a lot of energy was required to destroy the hydrogel network. To further investigate the injectability of the prepared hydrogel, the viscosity and shear thinning properties of PVA/CS/DES/-CuTA$_{500}$ hydrogels were studied. As shown in Fig. 2K and L, the viscosity of PVA/CS/DES/CuTA$_{500}$ hydrogel at different temperatures (25 °C and 37 °C) increased and then decreased with increasing shear rate. In addition, the compression properties of the prepared hydrogels were

further measured and quantified. As shown in Fig. S6, the compression modulus of the PVA/CS/DES/CuTA$_{500}$ hydrogel under 60 % compression strain is higher than 25 kPa, which is similar to the strength of physiological soft tissue. As shown in Fig. S7, the PVA/CS/DES/CuTA$_{500}$ hydrogel can still recover to the gel state after 20 cycles of 50 % compression strain, proving that the prepared hydrogel has certain fatigue resistance. These results confirmed that the hydrogel has good injectability, self-healing and adhesion properties and provides sufficient mechanical strength to promote the healing of infected wounds.

## 2.4. Swelling rate and water content of prepared hydrogels

Appropriate water content and structural stability help hydrogels maintain their functionality after contact with wound exudate in wound applications [21,46]. Swelling property is one of the important inherent characteristics of hydrogels, affecting the absorption of exudate from the wound site and the release effect of the drugs loaded in the hydrogel [47, 48]. The swelling rate of PVA/CS/DES/CuTA$_{250}$, PVA/CS/DES/-CuTA$_{500}$, and PVA/CS/DES/CuTA$_{1000}$ at different time points was tested. The prepared hydrogels swelled rapidly and reached a swelling equilibrium state within the first 2 h, and the swelling ratios of different hydrogels ranged from approximately 250 %–300 % (Fig. S8). In addition, the water content of the prepared hydrogels was further determined. The results showed no significant difference in the water content of all prepared hydrogels, which were over 80 % (Fig. S9). These results showed the prepared hydrogels' high absorption performance and stability, indicating that the hydrogels could effectively absorb exudate, maintain a moist environment at the wound site, and facilitate wound repair.

## 2.5. Release of TA and copper ions from prepared hydrogels

Folin-Ciocalteu (FC) reagent was used to evaluate the concentration of TA released from PVA/CS/DES/CuTA$_{500}$ and PVA/CS/DES/CuTA$_{1000}$ hydrogel. The results showed that in a liquid environment, the release of TA lasted for a long time and the concentration was low (no more than 30 µg mL$^{-1}$) (Fig. 2M). The local and sustained release of a small amount of copper ions is crucial for the hydrogels' safety and therapeutic effect in vivo [49]. Therefore, the concentration of copper ions released by PVA/CS/DES/CuTA$_{500}$ hydrogel in a liquid environment was tested by inductively coupled plasma mass spectrometry (ICP-MS). The results showed that the release of copper ions lasted for a long time, and a low concentration of copper ions (no more than 0.15 µg mL$^{-1}$) could still be detected on the 7th day (Fig. 2N). This sustained release mode could maintain copper ions at a low concentration and might be a feasible way to avoid unnecessary tissue toxicity.

## 2.6. In vitro antibacterial activity of prepared hydrogels

During wound recovery, bacterial infection will delay wound healing and is the main factor inducing severe inflammation [50]. Therefore, the ability of wound dressings to inhibit bacterial growth was the key to therapeutic efficacy. Gram-positive bacteria (S. aureus and MRSA) and Gram-negative bacteria (E. coli) were selected as representative bacteria to evaluate the in vitro antibacterial properties of the prepared hydrogels. First, the inhibition zone test was used to evaluate the antibacterial activity of the prepared hydrogels against S. aureus, MRSA, and E. coli (Fig. 3A and C). The results showed that obvious inhibition zones were observed around all prepared hydrogels, and the antibacterial effect became more obvious with the increase in CuTA concentration. In addition, the antibacterial effect of the prepared hydrogels was further evaluated using the plate counting method. As shown in Fig. 3B, many bacterial colonies were seen in the control group, and the bacterial colonies were reduced in the PVA/CS/DES group. This was mainly due to the antibacterial effect of CS and choline chloride, a component of DES [51]. Importantly, all PVA/CS/DES/CuTA hydrogels showed
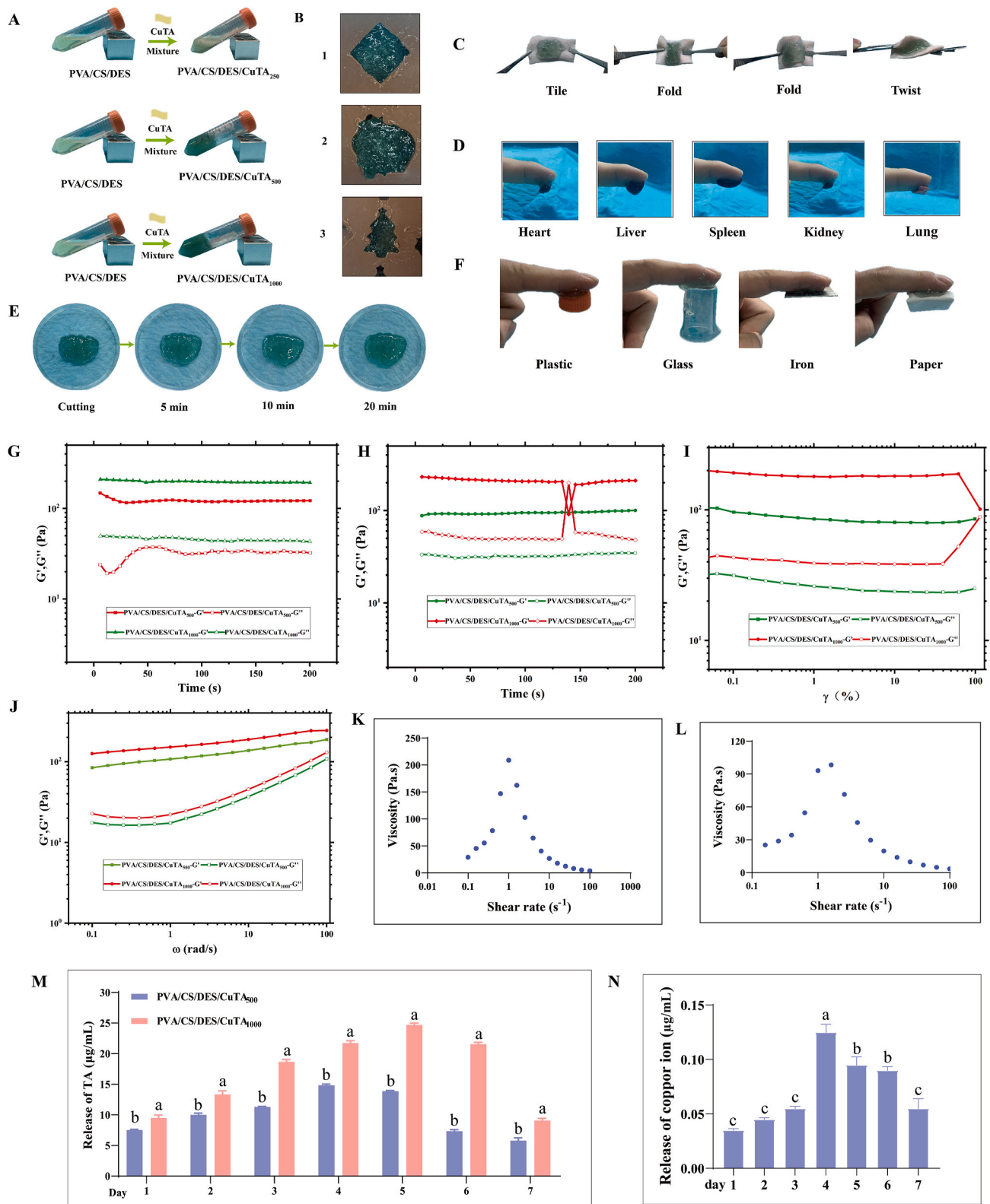
**Fig. 2.** Characterization of prepared hydrogels. (**A**) Photograph displaying the formation process of PVA/CS/DES/CuTA hydrogels. (**B**) Shape adaptability of PVA/CS/DES/CuTA$_{500}$ hydrogel. (**C**) Adhesion of PVA/CS/DES/CuTA$_{500}$ hydrogel to fresh porcine skin and its tiling, folding, and twisting. (**D**) Adhesion of PVA/CS/DES/CuTA$_{500}$ hydrogel to various organs (heart, liver, spleen, kidney, and lung) of mice. (**E**) The self-healing of PVA/CS/DES/CuTA$_{500}$ hydrogel. (**F**) Adhesion of PVA/CS/DES/CuTA$_{500}$ hydrogel on multiple materials (plastic, glass, paper, and iron). (**G-J**) Rheological properties of PVA/CS/DES/CuTA hydrogel as a function (strain of 0.5 %, ω = 6.28 rad s$^{-1}$). (**K and L**) Viscosity and shear thinning property of PVA/CS/DES/CuTA$_{500}$ hydrogel at different temperatures (25 °C and 37 °C). (**M and N**) TA and copper ion release from PVA/CS/DES/CuTA hydrogel (n = 3, mean ± SD).
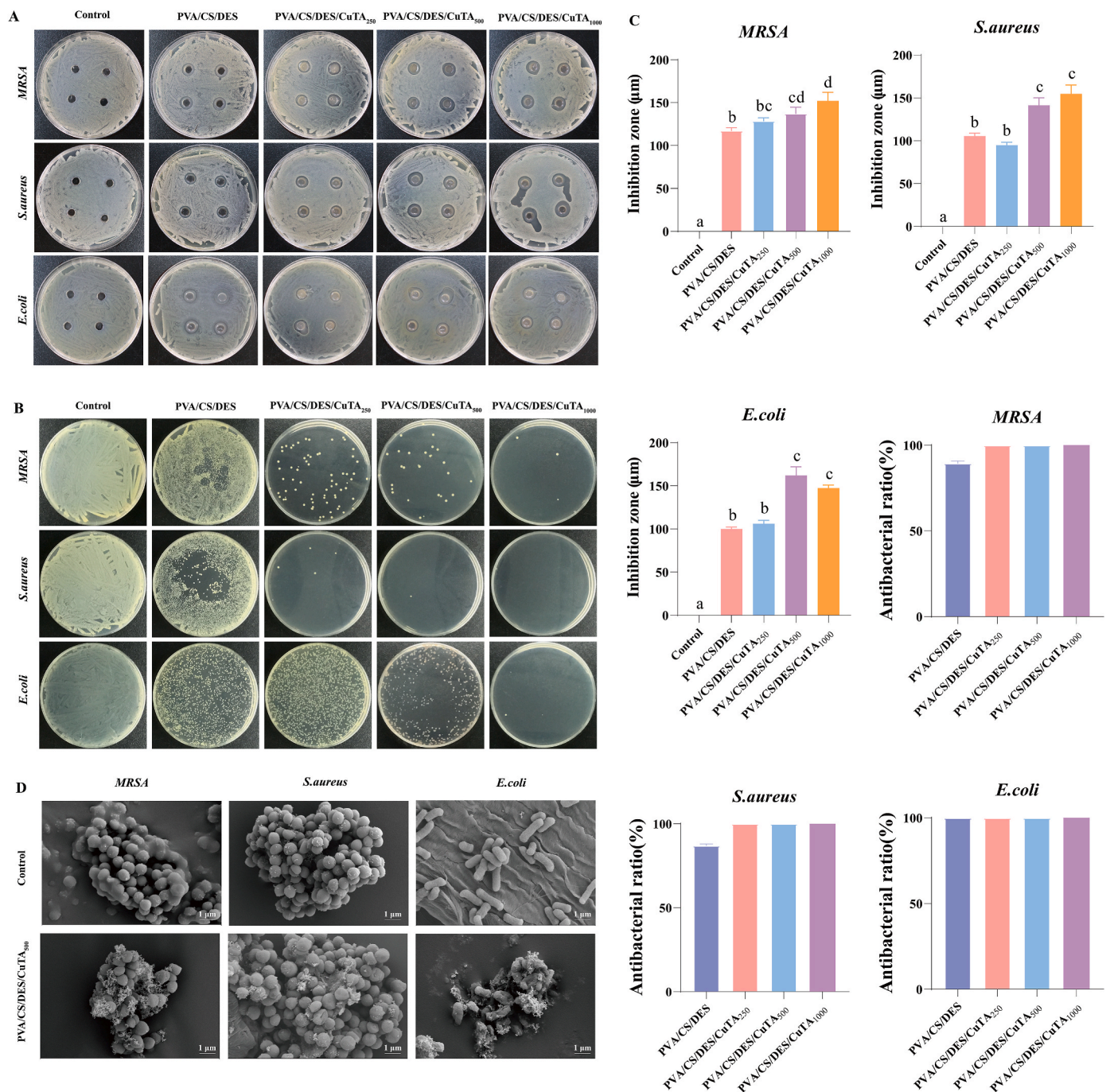
**Fig. 3.** Evaluation of the antibacterial activity of prepared hydrogels *in vitro*. (**A**) Images of inhibition zones against *MRSA*, *S. aureus*, and *E. coli*. with the control group (PBS) and different hydrogels. (**B**) Optical images of colonies after co-culture of prepared hydrogels and various components with *MRSA*, *S. aureus,* and *E. coli*. (**C**) Inhibition zones and antibacterial ratio of *MRSA*, *S. aureus*, and *E. coli* after treatment with different hydrogels. (**D**) SEM image of *MRSA*, *S. aureus*, and *E. coli* treated with PVA/CS/DES/CuTA$_{500}$ hydrogel. In all experiments, the data are mean $\pm$ SD, n = 3, the same letters represent no significant difference between the groups, and different letters represent significant differences between the groups. $p \leq 0.05$.

excellent antibacterial activity. As the CuTA content in the hydrogel increased, a gradual decrease in bacterial colonies was observed on the hydrogel-treated agar plate, indicating that the antibacterial properties of the hydrogel were significantly enhanced. This result was also verified by calculating the antibacterial rate. The antibacterial rate of PVA/CS/DES/CuTA$_{250}$, PVA/CS/DES/CuTA$_{500}$, and PVA/CS/DES/-CuTA$_{1000}$ hydrogels was close to 100 % (Fig. 3C). These results indicated the TA and copper ions endowed the hydrogel with better antibacterial properties, which was extremely important for infected wound healing.

To further explore the antibacterial mechanism of prepared hydrogel

against *S. aureus*, *MRSA*, and *E. coli*. Therefore, SEM was used to observe the morphological changes of bacteria after co-culture with PVA/CS/DES/CuTA$_{500}$ hydrogel. As shown in Fig. 3D, the bacterial surface of *MRSA*, *S. aureus*, and *E. coli* in the control group was relatively smooth and intact, and no wrinkles or invagination were observed. On the contrary, after the three bacteria were co-cultured with PVA/CS/DES/CuTA$_{500}$ hydrogel, it was seen that most of the bacteria showed obvious cell structure collapse, shrinkage, or even rupture into fragments, accompanied by a large amount of cell-matrix leakage. These results highlighted the excellent antibacterial properties of the prepared

hydrogel, confirming the potential for clinical application in the treatment of infected wounds. Based on these results, the antibacterial mechanism of the hydrogels may involve the following factors. The abundant cationic groups in the hydrogels (such as choline chloride and chitosan) could bind to the negatively charged bacterial membranes, thereby breaking up the bacterial membranes [52,53]. Free phenolic hydroxyl groups such as TA capture bacteria as they approach, resulting in cell membrane rupture and leakage of cell contents [26,40]. In addition, copper ions released from the hydrogels can easily change the potential balance on the bacterial membranes, inhibit DNA replication, hinder bacterial metabolism, induce cytoplasmic leakage, and ultimately lead to bacterial cell death [36]. Therefore, the combination of all the above mechanisms significantly improved the antibacterial properties of the prepared hydrogel, indicating its great potential for application in clinically infected wounds.

### 2.7. Cytocompatibility and cell migration assays of prepared hydrogels

Good cytocompatibility is essential for hydrogels' application in clinical wound dressings [54]. The in vitro cytocompatibility of hydrogel extracts was evaluated using the cell counting kit-8 (CCK-8) kit and Live/Dead staining. First, L929 cells were cultured in different concentrations (0, 7.5, 15, and 30 mg mL$^{-1}$) of PVA/CS/DES/CuTA$_{250}$, PVA/CS/DES/CuTA$_{500}$, and PVA/CS/DES/CuTA$_{1000}$ hydrogel extracts for 24 h, and then the cell viability was determined using the CCK-8 kit. As shown in Fig. 4A, at a hydrogel concentration of 7.5 mg mL$^{-1}$, the cell viability of L929 cells treated with 50 % hydrogel extract exceeded 100 % compared with the control group, indicating that the prepared hydrogel was relatively non-cytotoxic. Similarly, similar results were obtained after HUVEC cells were treated with hydrogel extracts of different concentrations for 24 h (Fig. S11). Subsequently, Live/Dead staining was used to observe the cell survival after 24 h of culture with 50 % dilution of the hydrogel extract at a concentration of 7.5 mg mL$^{-1}$ (Blue fluorescence represents live cells, and red fluorescence represents dead cells.). The results showed that a large amount of blue fluorescence was visible after 24 h of culture for all hydrogels, and there was almost no red fluorescence, further indicating that the prepared hydrogel had no obvious cytotoxicity to L929 cells (Fig. 4B). Afterwards, CCK-8 was also performed on L929 cells with different gradient concentrations of PVA/CS/DES/CuTA$_{250}$ and PVA/CS/DES/CuTA$_{500}$ hydrogel extracts at a concentration of 7.5 mg mL$^{-1}$ (Fig. 4C). The results showed that 50 % of the hydrogel extracts and their concentrations below showed no significant toxicity to L929 cells according to the standard ISO 10993-5. Moreover, the scratch test was also used to evaluate the effect of 50 % hydrogel extracts (7.5 mg mL$^{-1}$) on cell migration. As shown in Fig. 4D, after incubation with the hydrogel extract for 48 h, the scratch area of the PVA/CS/DES/CuTA$_{250}$ and PVA/CS/DES/CuTA$_{500}$ hydrogel extract groups was significantly reduced. Compared with the control group (~50 %), the PVA/CS/DES/CuTA$_{500}$ hydrogel group showed an excellent scratch healing rate (over 85 %) ($p < 0.05$) (Fig. 4F). The above results further confirmed that the prepared hydrogels had excellent cell compatibility and migratory properties.

### 2.8. Hemocompatibility and hemostasis assays of prepared hydrogels

Blood compatibility is one of the important indicators for evaluating medical materials in biomedical applications [55]. According to ASTM F756-00, biomedical materials with a hemolysis rate (HR) not exceeding 5 % are considered blood-compatible [1]. Therefore, the blood compatibility of various hydrogels was evaluated by hemolysis experiment. Deionized water (DW) was used as the positive control group, and PBS was used as the negative control group. The results showed that no obvious hemolysis occurred in the PVA/CS/DES/CuTA$_{250}$ and PVA/CS/DES/CuTA$_{500}$ hydrogels group, and the HR were all less than 5 %, indicating that the hydrogel has good blood compatibility and could be further safely used as clinical wound dressings (Fig. 4E).

Hemostasis is an important stage in wound healing and is indispensable for subsequent wound repair. Moreover, wound dressings with excellent hemostatic properties have attracted more attention [56]. Initially, the liver bleeding model and a tail amputation bleeding model of mice were constructed to evaluate the hemostatic effect of the prepared hydrogels. Fig. 4G was a schematic diagram of the mouse liver and tail bleeding model. In the liver bleeding model, the maximum blood loss in the blank group was approximately 0.142 g. In contrast, the blood loss after hydrogel treatment was lower, about 0.039 g and 0.023 g, respectively, and was better than medical gauze (~0.043 g) and showed a significant hemostatic effect (Fig. 4H). Similarly, similar results were obtained in the tail bleeding model (Fig. 4I). The above results confirmed that the prepared hydrogels had excellent hemostatic ability. Furthermore, the blood clotting index (BCI) was used to determine the in vitro coagulation performance of the prepared hydrogels. The level of BCI represents the coagulation speed after the hydrogel comes into contact with blood [57]. As shown in Fig. 4K, compared with the control group, the PVA/CS/DES/CuTA$_{250}$ group, and the PVA/CS/DES/CuTA$_{500}$ group observed clear blood coagulation, with only a small amount of uncoagulated red blood cells remaining after resuspension, and the BCI were approximately 11.61 % and 15.02 %, respectively. These results confirmed the superior hemostatic and coagulation properties of the prepared hydrogel. The hydrogels with adhesive properties could perfectly cover the bleeding wound, and the internal pores could absorb the blood exuded from the wound [58]. In addition, the positively charged substances in the hydrogel, such as CS and choline chloride, could attract platelet aggregation and activate the coagulation pathway [59,60]. The polyphenol groups in CuTA in the hydrogel could interact with blood proteins and aggregate calcium ions, thereby accelerating blood coagulation [61]. Therefore, the prepared hydrogels could provide hemostasis and rapid coagulation in the early stage of wound healing.

### 2.9. In vivo biocompatibility evaluation

To investigate the in vivo biocompatibility of PVA/CS/DES/CuTA$_{500}$ hydrogel, the hydrogel was injected subcutaneously into the back of mice, and the skin tissues surrounding the hydrogel were histopathologically analyzed. 7 days after subcutaneous injection, H&E staining of the skin tissues around the hydrogel showed that the implanted hydrogel was degraded into fragments, and no obvious inflammatory cell infiltration and tissue necrosis were observed around the hydrogel, indicating the inflammatory response at the hydrogel-tissue interface decreased significantly. (Fig. S12). Next, Masson staining was performed to determine collagen deposition around the hydrogel implantation site, which can be used as an indicator of fibrous wrapping around the implant, thus reflecting a foreign body reaction (FBR) [62]. The results showed that sparse collagen fibers were observed 7 days after implantation, with only a small amount of collagen fibers wrapped around PVA/CS/DES/CuTA$_{500}$ hydrogel. Finally, the main organs (heart, liver, spleen, lung, and kidney) were collected and analyzed by H&E staining. The results showed that no obvious pathological changes were observed in the organs of the hydrogel-treated group compared with the control group, indicating that PVA/CS/DES/CuTA$_{500}$ hydrogel has good biosafety in vivo (Fig. S13).

### 2.10. Evaluation of hydrogel on acute skin wound healing

Preliminary experimental results confirmed that the prepared hydrogel has excellent biocompatibility, tissue adhesion, and hemostatic properties. Therefore, the healing effect of PVA/CS/DES/CuTA$_{500}$ hydrogel in a mouse acute skin wound model was further evaluated. A wound was constructed on the back of normal mice using a skin biopsy punch and then treated with PVA/CS/DES/CuTA$_{500}$ hydrogel, Duo-DERM hydrogel, or saline (control group), respectively. The treatment process was carried out according to the schedule shown in Fig. 5A. As
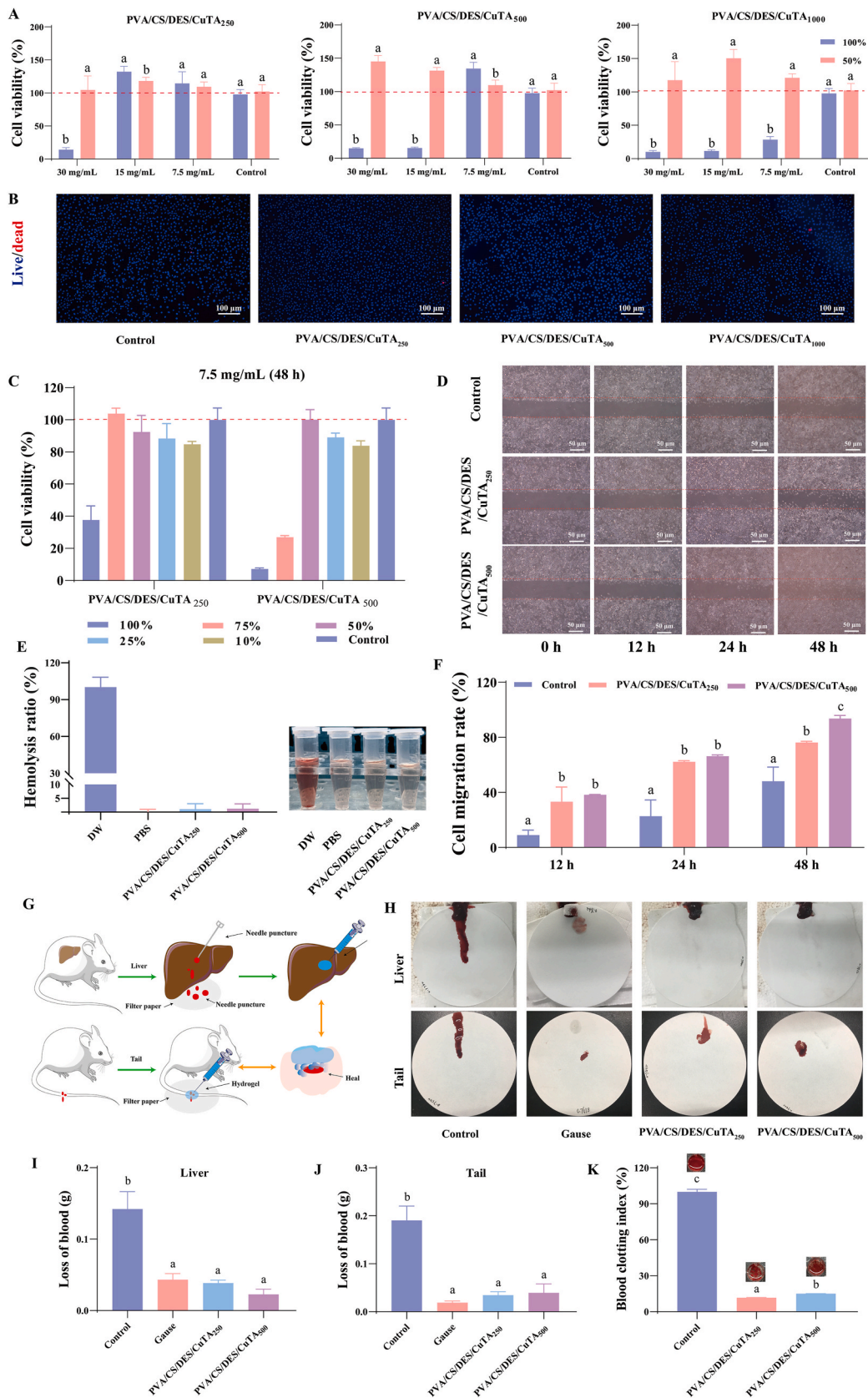
**Fig. 4.** Evaluation of biocompatibility and hemostatic properties of prepared hydrogels. (**A**) L929 cells were incubated with extracts from prepared hydrogels for 24 h to measure cell viability. (**B**) Live/dead staining of L929 cells treated with different hydrogels after 24 h (blue: live cells; red: dead cells). (**C**) L929 cells were incubated with extracts from prepared hydrogels for 48 h to measure cell viability. (**D**) Representative optical images of cell migration after co-culture of the prepared hydrogel extracts with L929 cells. (**E**) Hemolysis test of the prepared hydrogels. (**F**) Quantitative analysis of wound closure rate in a scratch assay. (**F**) Quantitative analysis of cell migration rate in a scratch assay. (**G**) Schematic diagram of liver and tail bleeding models. (**H**) Representative blood stain photos of hydrogels used in the mouse liver and tail bleeding models. (**I and J**) Statistical analysis of blood loss after hydrogel treatment in the mouse liver and tail bleeding model. (**K**) Blood clotting index (BCI%) of different hydrogels. In all experiments, the data are mean $\pm$ SD, n = 3, the same letters represent no significant difference between the groups, and different letters represent significant differences between the groups. $p \leq 0.05$.

shown in Fig. 5B, after 3 days of treatment, the wounds of mice in each group gradually shrank. Compared with the control group (~27.42 %), the wound healing effect of mice treated with PVA/CS/DES/CuTA$_{500}$ hydrogel and DuoDERM hydrogel was the most obvious, with wound area healing of approximately 70.11 % and 58.51 %, respectively (Fig. 5F).

To further evaluate the wound healing, H&E staining, and Masson staining were performed on the skin tissue in the wound area. The results showed that the wounds of mice in control and DuoDERM groups had acute inflammatory reactions, many inflammatory cells accumulated near the wounds, and many wound defects were observed without a complete epidermis. However, the inflammatory infiltration in the wound area of the PVA/CS/DES/CuTA$_{500}$ group was milder, with a small amount of epidermis formation, and the wound propria was relatively intact (Fig. 5C). In addition, the collagen deposition evaluated by Masson staining showed that compared with the control group, PVA/CS/DES/CuTA$_{500}$ showed obvious collagen deposition after treatment, indicating that PVA/CS/DES/CuTA$_{500}$ hydrogel has a superior wound healing effect (Fig. 5D). To further investigate the inflammatory status during acute wound healing, the expression levels of IL-10 (anti-inflammatory signal) and TNF-α (pro-inflammatory signal) in wound tissues were detected by immunofluorescence (Fig. 5E). The results showed that compared with the control group, TNF-α was significantly down-regulated and IL-10 was significantly up-regulated in the PVA/CS/DES/CuTA$_{500}$ group. In contrast, the two signals in the DuoDERM-treated wound area showed moderate expression (Fig. 5G and H). In general, the above research results showed that PVA/CS/DES/CuTA$_{500}$ hydrogel effectively promoted the healing of acute skin wounds in mice, mainly by reducing inflammatory responses. Next, the effect of PVA/CS/DES/CuTA$_{500}$ hydrogel was evaluated in difficult-to-heal *MRSA*-infected wounds, in which bacterial infection was severe, inflammatory infiltration was abundant, and poor neovascularization.

### 2.11. Evaluation of hydrogel on MRSA-infected wound healing

To evaluate the therapeutic effect of PVA/CS/DES/CuTA$_{500}$ hydrogel on more challenging, non-healing wounds, an *MRSA*-infected full-thickness skin wound model (diameter: 6 mm) was established in mice, in which wound healing was significantly delayed due to severe inflammation and limited angiogenesis [63,64]. The specific experimental steps were carried out according to the schematic diagram shown in Fig. 6A. After establishing *MRSA*-infected wounds, they were treated with saline (negative control), DuoDERM (positive control), or PVA/CS/DES/CuTA$_{500}$ hydrogel. As shown in Fig. 6B and C, after 7 days of treatment, a large area of obvious scabs and pus exudation was observed on the surface of the wounds in the *MRSA* group compared with the control group, indicating the wound healing of *MRSA* infection was delayed. However, after intervention with PVA/CS/DES/CuTA$_{500}$ hydrogel, the scab at the wound completely fell off, the wound surface was smooth and new granulation tissue was generated. The therapeutic effect was similar to that of the DuoDERM group. Similarly, the wound healing rates of the PVA/CS/DES/CuTA$_{500}$ hydrogel and DuoDERM hydrogel groups were approximately 81.30 % and 71.71 % respectively, which were significantly higher than that of the *MRSA* group (~28.42 %) (Fig. 6K). The main reason was the good adhesion, hemostasis, and antibacterial properties of PVA/CS/DES/CuTA$_{500}$ hydrogel, providing an excellent environment for *MRSA*-infected wound healing.

To further investigate the actual healing effect of PVA/CS/DES/CuTA$_{500}$ hydrogel on *MRSA*-infected wounds, H&E staining, and Masson staining were used to examine histological analysis of wound tissues. Due to bacterial infection, fibroblasts and inflammatory cells are recruited in large numbers in the initial stage of wound healing, leading to severe acute inflammatory response [45,65]. As shown in Fig. 6D–H&E staining results showed the infected wounds in the *MRSA* group still had a strong inflammatory reaction on day 7, with obvious scabs at the wound surface, severe wound defects, and massive inflammatory cell infiltration, which may prolong the inflammatory period and hinder wound healing. Compared with the *MRSA* group, wound tissue treated with PVA/CS/DES/CuTA$_{500}$ hydrogel showed reduced inflammatory cell infiltration, smaller granulation gaps, and shorter wound area length on day 7 (Fig. 6G and H). It's known that collagen deposition and arrangement are important indicators of wound healing [66]. Masson staining showed that bacterial-infected wounds treated with hydrogels had more collagen fibers. In contrast, the *MRSA* group had fewer collagen fibers, indicating that the PVA/CS/DES/CuTA$_{500}$ hydrogel could increase collagen deposition (Fig. 6E and I). In addition, the *in vivo* antibacterial effect of the hydrogel was evaluated, and results showed that PVA/CS/DES/CuTA$_{500}$ hydrogel inhibited the reproduction of bacteria in the infected wound and had good bactericidal activity (Fig. 6F and J). In summary, the above results demonstrated PVA/CS/DES/CuTA$_{500}$ hydrogel could accelerate infected wound healing by inhibiting bacterial growth, reducing the inflammatory response, and promoting collagen deposition.

### 2.12. Pro-angiogenesis and anti-inflammatory effects of prepared hydrogel in vivo

Persistent severe inflammation in the skin wound area is a significant challenge that delays healing [67]. Macrophages are crucial in the wound recovery process, and the polarization of their phenotype from M1 to M2 is the key to the transition from the inflammatory phase to the proliferation phase [68]. To evaluate the anti-inflammatory properties of PVA/CS/DES/CuTA$_{500}$ hydrogel *in vivo*, immunofluorescence analysis of wound tissue was performed on day 7 (F480/CD86 marked M1 macrophages; F480/M2 marked macrophages) (Fig. 7A). In the *MRSA* group, M1 macrophages (F480/CD86) were dominant, and the fluorescence intensity was significantly higher than that in the PVA/CS/DES/CuTA$_{500}$ hydrogel and DuoDREM groups. However, the expression trend of M2 macrophages (F480/CD206) was the opposite, significantly lower than that of other groups, indicating that the wound environment of the *MRSA* group was still in the inflammatory stage caused by bacterial infection. In the PVA/CS/DES/CuTA$_{500}$ hydrogel group, the excellent antibacterial properties of the prepared hydrogel helped eliminate inflammation, and the inherent self-healing properties of the hydrogel were conducive to matching irregular wounds, thereby reducing inflammatory responses. Therefore, compared with the *MRSA* group, the immunofluorescence intensity of the M2 phenotype marker F480/CD206 increased significantly in the DuoDERM and PVA/CS/DES/CuTA$_{500}$ hydrogel groups, with the most obvious fluorescence intensity observed in the PVA/CS/DES/CuTA$_{500}$ hydrogel group. The immunomodulatory function of the prepared hydrogel might be attributed to the sustained release of CuTA, which was essential for bacterial elimination. In addition, the TA in CuTA in the prepared hydrogel also had an anti-inflammatory effect. Bacterial-infected wounds also usually
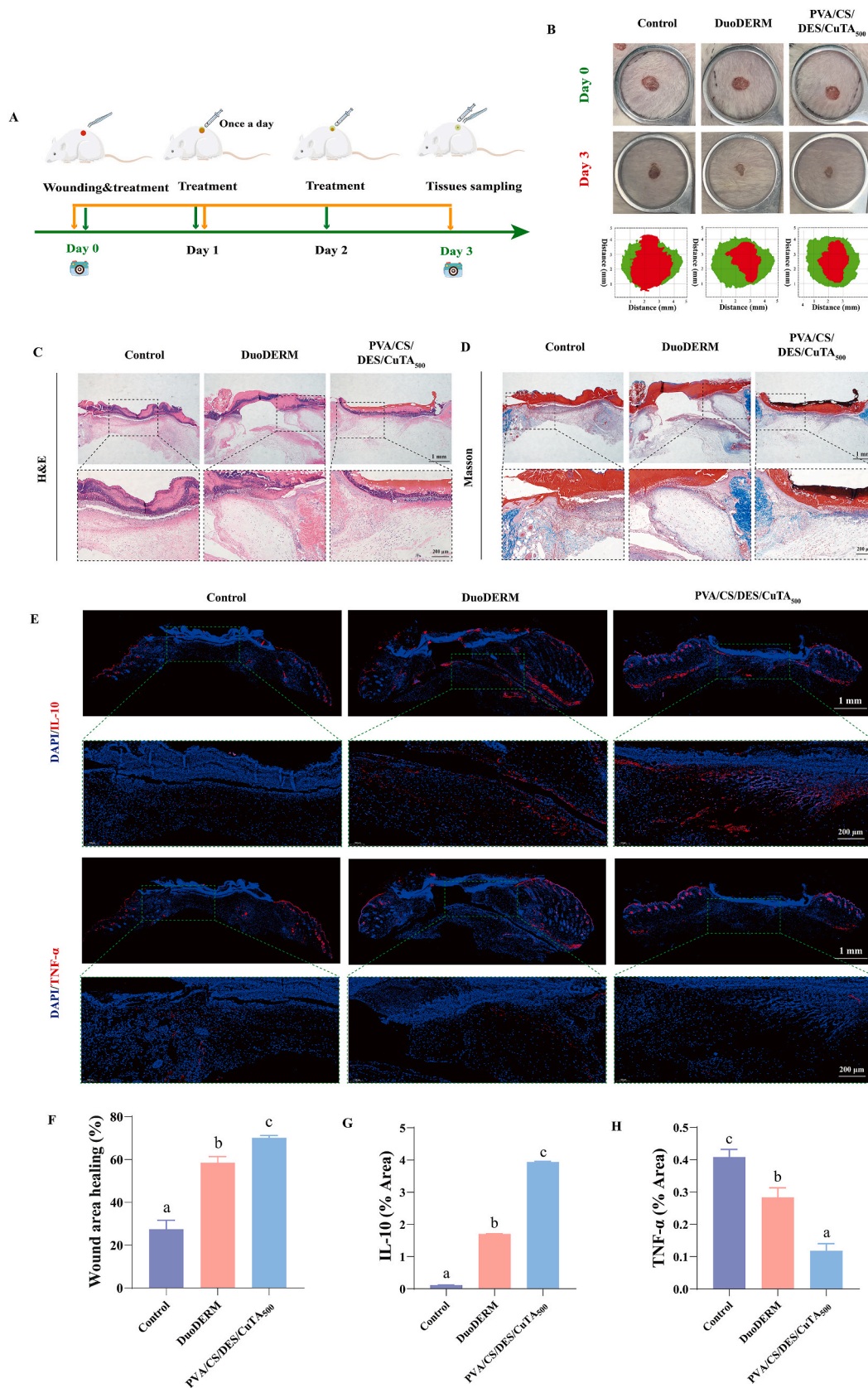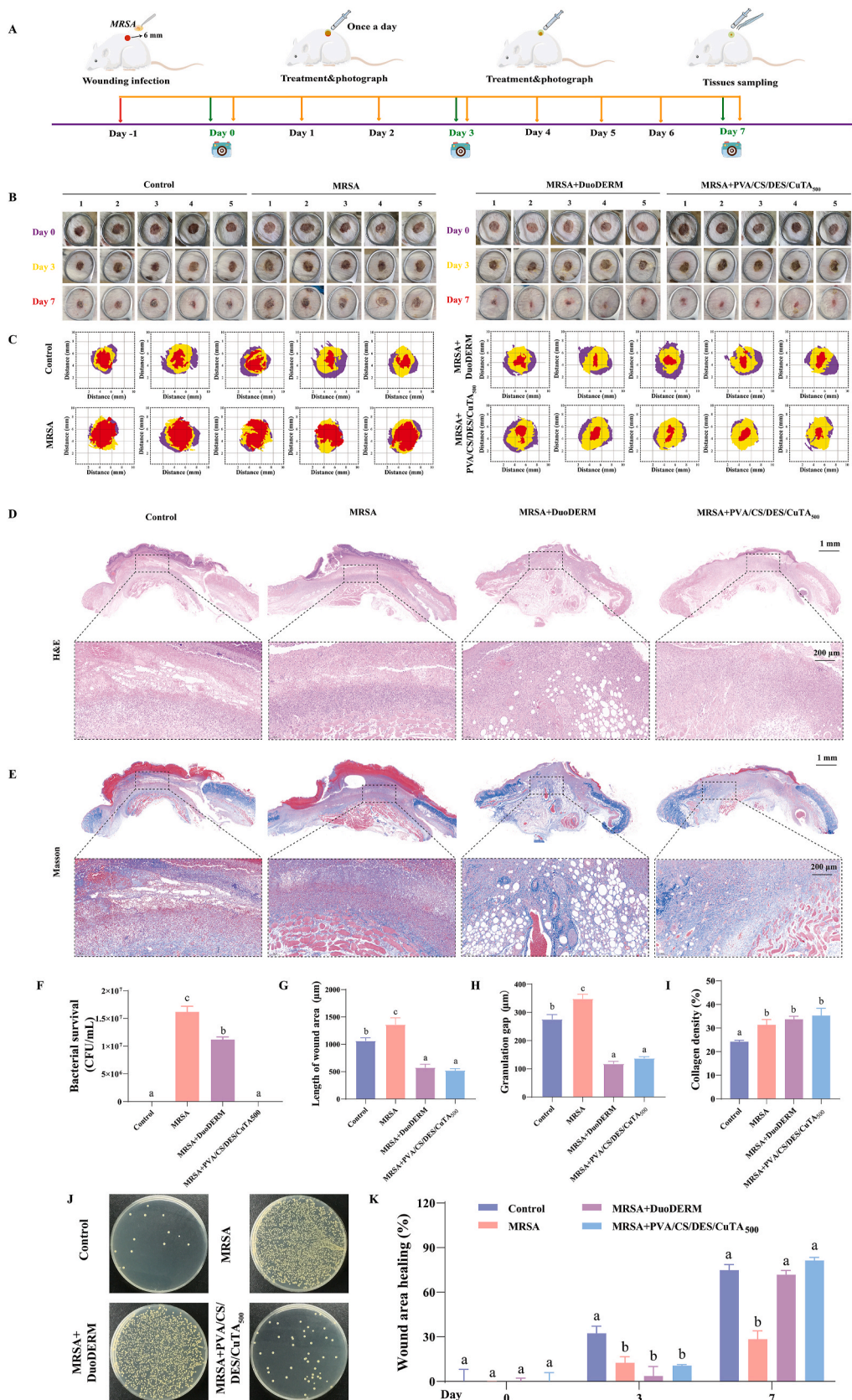
**Fig. 5.** PVA/CS/DES/CuTA$_{500}$ hydrogel promotes acute skin wound healing. (**A**) Schematic diagram of acute skin wound model and treatment scheme. (**B**) Representative skin wound images during wound healing and simulations of wound areas at different times. (**C** and **D**) Images of regenerated skin after H&E and Masson`s trichrome staining. (**E**) Representative image of IL-10 and TNF-α in wound tissues. (**F**) Quantitative analysis of relative wound healing. (**G** and **H**) Fluorescence intensity ratio of immunofluorescence of IL-10 and TNF-α in wound tissues. In all experiments, the data are mean ± SD, n = 3, the same letters represent no significant difference between the groups, and different letters represent significant differences between the groups. $p \leq 0.05$.

*(caption on next page)*

**Fig. 6.** PVA/CS/DES/CuTA$_{500}$ hydrogel promotes the healing of *MRSA*-infected skin wounds. (**A**) Schematic diagram of *MRSA*-infected wound model and treatment process. (**B**) Representative images of wounds during the infected wound healing process. (**C**) Simulation of wound area at different times during treatment. (**D** and **E**) Image of skin wound after H&E and Masson's trichrome staining. (**F**) Statistics of bacterial survival in infected wounds. (**G**–**I**) Quantitative analysis of wound area length, granulation gap, and collagen density in the wound area. (**J**) Representative image of bacterial colonies in an infected wound. (**K**) Quantitative analysis of relative wound area healing. In all experiments, the data are mean ± SD, n = 3, the same letters represent no significant difference between the groups, and different letters represent significant differences between the groups. $p \leq 0.05$.

produce severe inflammatory responses. IL-6 is a common pro-inflammatory factor, while TGF-β is an anti-inflammatory factor, and is important for wound healing [67,69]. Therefore, the degree of wound inflammation was evaluated by testing the expression of IL-6 and TGF-β. As shown in Fig. 7B, IL-6 expression was significantly increased and TGF-β expression was significantly decreased in the *MRSA* group. However, the intervention of PVA/CS/DES/CuTA$_{500}$ hydrogel reversed this trend, showing down-regulation of IL-6 expression and up-regulation of TGF-β expression, supporting the excellent anti-inflammatory effect of PVA/CS/DES/CuTA$_{500}$ hydrogel.

After the wound transitions from the inflammatory phase to the proliferative phase, sufficient nutrients are needed to promote proliferation and repair, and new blood vessels are important channels for the transport of substances during the formation of epithelial tissue [36]. CD31 is a transmembrane protein expressed in endothelial cells, while α-smooth muscle actin (α-SMA) is a marker of smooth muscle cells in mature blood vessels. Therefore, double immunofluorescence staining of CD31 and α-SMA was performed to evaluate neovascularization (Fig. 7C). The results showed that compared with the *MRSA* group, the fluorescence expression of α-SMA (green) and CD31 (red) in the wound tissue after PVA/CS/DES/CuTA$_{500}$ hydrogel intervention was stronger. More mature new blood vessels were seen in the prepared hydrogel group, indicating that PVA/CS/DES/CuTA$_{500}$ hydrogel significantly promoted the early formation of new blood vessels in infected wounds. To further study the potential mechanism of PVA/CS/DES/CuTA$_{500}$ promoting angiogenesis, double immunofluorescence staining of HIF-1α and VEGF in wound tissue was detected. As shown in Fig. 7D, green fluorescence represented the positive expression of HIF-1α. The fluorescence intensity was almost invisible in the *MRSA* group. However, the PVA/CS/DES/CuTA500 hydrogel group shows the highest fluorescence intensity, which might be attributed to the stabilizing effect of Cu$^{2+}$ released from the hydrogel on HIF-1α [70]. Importantly, HIF-1α also increases the transcriptional activity of VEGF, thereby promoting neovascularization [36]. The expression of VEGF also increased significantly after PVA/CS/DES/CuTA$_{500}$ hydrogel treatment, confirming the promoting effect of HIF-1α on VEGF transcription. Interestingly, the increased expression of HIF-1α in the PVA/CS/DES/CuTA$_{500}$ hydrogel group was not as obvious as the upregulation of VEGF expression, indicating that HIF-1α was not the only promoter of VEGF expression. We speculated that PVA/CS/DES/CuTA$_{500}$ hydrogel might promote the polarization of macrophages into M2 macrophages during wound healing, and secreted VEGF to stimulate angiogenesis, ultimately accelerating wound healing [71].

### 2.13. Possible mechanism by which the hydrogel promoted wound healing

To systematically elucidate the potential mechanism of PVA/CS/DES/CuTA$_{500}$ hydrogel on the healing of infected wounds, wound tissue samples were collected 7 days after treatment for RNA sequencing (RNA-seq). The differentially expressed genes caused by different treatment groups could be seen from the co-expression Venn diagram (Fig. S14). Specifically, as shown in the volcano plot and thermal maps, compared with the control group, the *MRSA* group had 45 up-regulated and 576 down-regulated differentially expressed genes (DEGs) at 7 days after surgery. However, there were 283 DEGs between the PVA/CS/DES/CuTA$_{500}$ hydrogel group and the *MRSA* group, including 210 up-regulated genes and 73 down-regulated genes (fold change ≥2, $P <$ 0.05) (Figure S15 and Fig. 8A). The hierarchical clustering analysis heat

map of the three groups of DEGs showed that the expression patterns of the control group and the PVA/CS/DES/CuTA$_{500}$ hydrogel group were roughly consistent, but were significantly different from the *MRSA* group. However, between the prepared hydrogel-treated group and the *MRSA* group, most DEGs showed a reverse regulatory trend (Fig. 8B). Next, GO enrichment analysis was performed to determine the main biological functions of the top-ranked differentially expressed genes. Classification was performed based on the enrichment score, and the results showed the top 10 most relevant GO terms ($P < 0.05$). As shown in Fig. 8C and D, the most abundant ones were mainly molecular function terms, which included cytokine receptor binding, signaling receptor binding, molecular transducer activity signaling receptor activity, cytokine activity, tumor necrosis factor receptor superfamily binding, and signal transducer activity. Additionally, the results of KEGG enrichment analysis showed that DEGs were mainly enriched in cytokine-cytokine receptor interaction, NF-kappa B signaling pathway, NOD-like receptor signaling pathway, TNF signaling pathway, and other inflammation-related pathways (Fig. 8E and F). The above results of the KEGG enrichment analysis confirmed that PVA/CS/DES/CuTA$_{500}$ hydrogel could promote the healing of infected wounds by inhibiting inflammation-related pathways.

### 3. Conclusions

This study constructed a new injectable multifunctional hydrogel based on PVA and CS and evaluated its potential to promote the healing of acute and infected wounds. PVA/CS/DES/CuTA$_{500}$ hydrogel was prepared by a one-step mixing method, which was maintained by cross-linking of natural DES, PVA, CS, TA, and Cu$^{2+}$ through non-covalent interactions and metal coordination. PVA/CS/DES/CuTA$_{500}$ hydrogel had multifunctional properties, including injectability, good tissue adhesion, excellent biocompatibility, hemostatic properties, and broad-spectrum antibacterial properties. It was worth emphasizing that PVA/CS/DES/CuTA$_{500}$ hydrogel accelerated the healing of *MRSA*-infected wounds by killing bacteria, activating M2 polarization, anti-inflammation, and promoting angiogenesis. Taken together, PVA/CS/DES/CuTA$_{500}$ hydrogel had great potential for application in bacterial-infected wound treatment. However, some limitations need to be considered in this study. First, the antibacterial mechanism of the prepared hydrogels needs to be further explored, such as bacterial transcriptome sequencing. Secondly, the release of active ingredients in the prepared hydrogels under different pH environments should be considered to explore whether they are pH responsive. Therefore, in subsequent studies, we will focus on exploring the above two aspects to further improve the treatment strategy for bacterially infected wounds.

### CRediT authorship contribution statement

**Ruigang Zhou:** Writing – review & editing, Writing – original draft, Methodology, Investigation, Formal analysis, Data curation, Conceptualization. **Junjie Huang:** Writing – review & editing, Conceptualization, Data curation, Formal analysis, Methodology. **Wenhai Zhang:** Writing – review & editing. **Weimei Wang:** Writing – review & editing. **Weilong Peng:** Writing – review & editing. **Jun Chen:** Writing – review & editing. **Chenglong Yu:** Writing – review & editing. **Ruonan Bo:** Writing – review & editing. **Mingjiang Liu:** Writing – review & editing. **Jingui Li:** Writing – review & editing, Validation, Supervision, Funding acquisition, Formal analysis, Conceptualization.
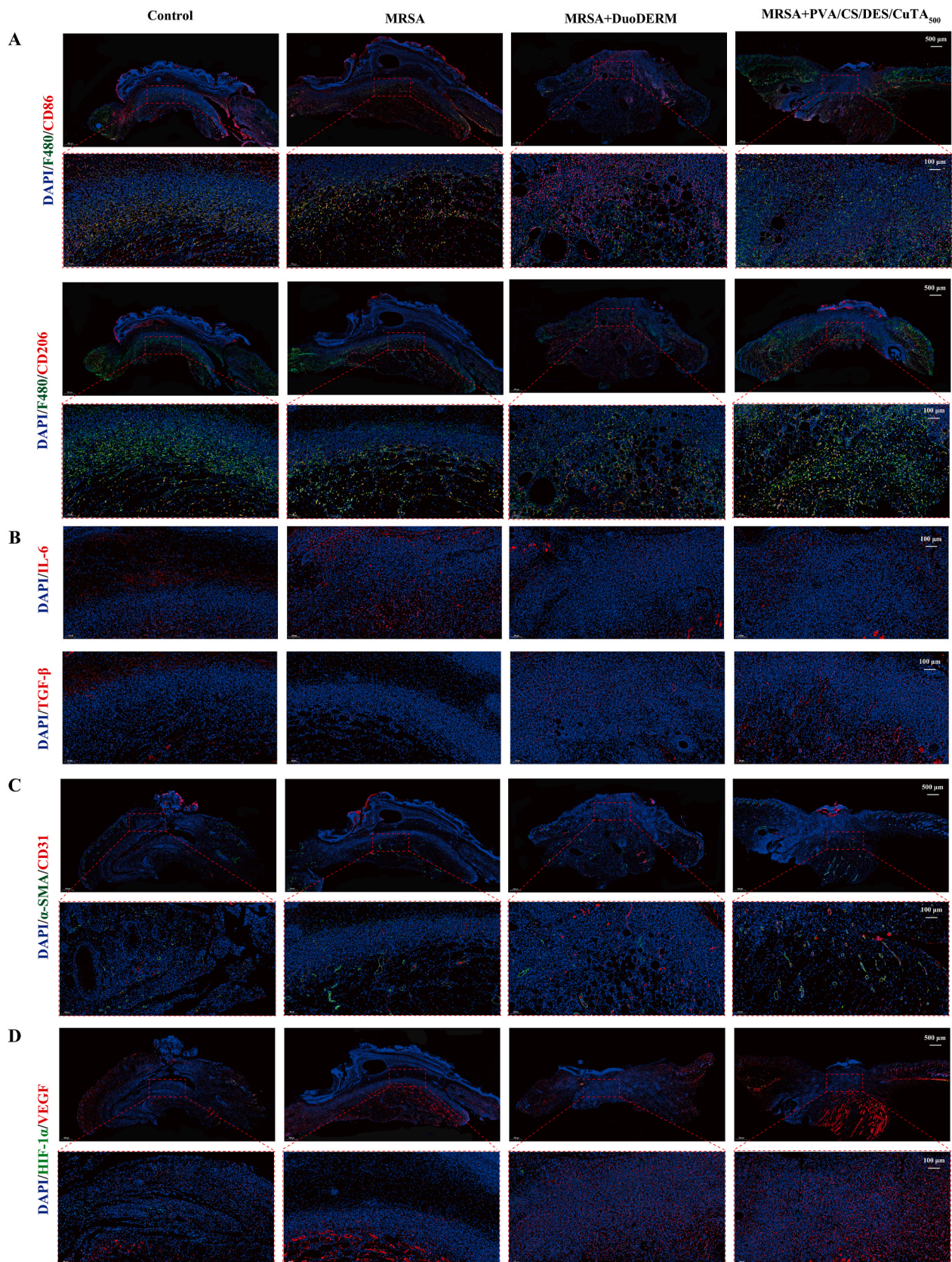
**Fig. 7.** Immunofluorescence staining of infected wound tissues to evaluate angiogenesis and anti-inflammatory effects *in vivo*. (**A**) Expression of CD86 and CD206 in different treatments of *MRSA*-infected wounds. (**B**) Expression of IL-6 and TGF-β in different treatments of *MRSA*-infected wounds. (**C**) Representative images of immunofluorescence of α-SMA and CD31 in infected wound tissue. (**D**) Representative images of HIF-1α and VEGF in wound tissues.
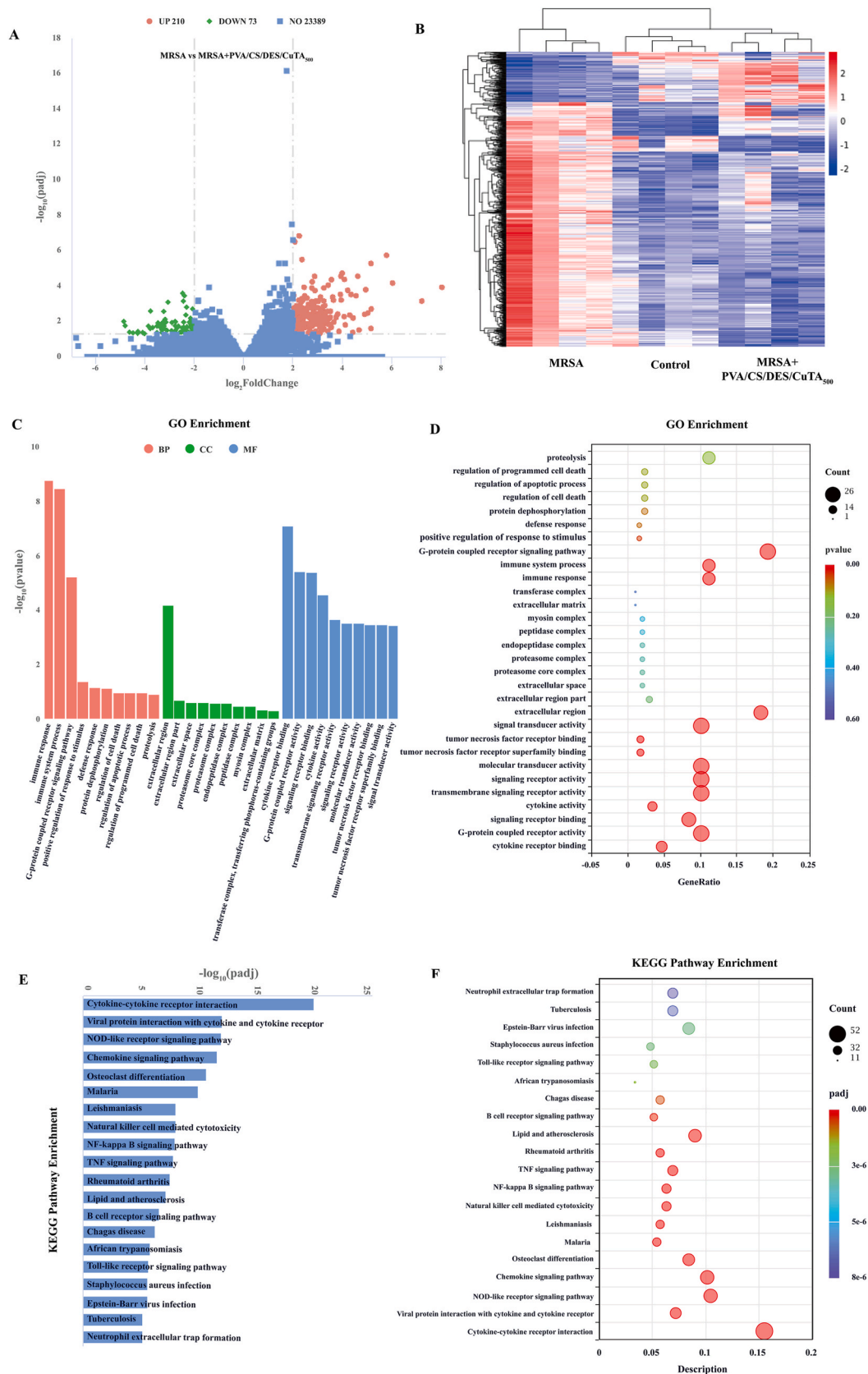
**Fig. 8.** RNA sequencing analysis of the regeneration mechanism of infected wounds. (**A**) Volcano plot depicting differentially expressed genes in the *MRSA* and PVA/CS/DES/CuTA$_{500}$ hydrogel groups. (**B**) Cluster analysis of skin wound tissue (n = 3). (**C** and **D**) Gene expression profiles of skin wound tissues were analyzed by Gene Ontology (GO). (**E** and **F**) KEGG pathway analysis showed the enrichment of relevant pathways. Abbreviations: BB, biological process; CC, cellular component; MF, molecular function. All experiments were repeated at least three times.

## Ethics approval

This study was conducted according to the guidelines approved by the Animal Care and Use Committee of Yangzhou University, China.

## Declaration of competing interest

The authors declare that they have no known competing financial interests or personal relationships that could have appeared to influence the work reported in this paper.

## Acknowledgements

## Appendix A. Supplementary data

Supplementary data to this article can be found online at https://doi.org/10.1016/j.mtbio.2024.101315.

## Data availability

Data will be made available on request.

## References

[1] Y. Duan, F. Jiang, Q. Li, A. McDowell, Y. Li, Y. Wang, S. Liu, C. Zhang, X. Pan, Multifunctional polysaccharide/metal/polyphenol double-crosslinked hydrogel for infected wound, Carbohydr. Polym. 332 (2024) 121912, https://doi.org/10.1016/j.carbpol.2024.121912.

[2] B. Guo, Y. Liang, R. Dong, Physical dynamic double-network hydrogels as dressings to facilitate tissue repair, Nat. Protoc. 18 (2023) 3322–3354, https://doi.org/10.1038/s41596-023-00878-9.

[3] P. Zhao, Y. Zhang, X. Chen, C. Xu, J. Guo, M. Deng, X. Qu, P. Huang, Z. Feng, J. Zhang, Versatile hydrogel dressing with skin adaptiveness and mild photothermal antibacterial activity for methicillin-resistant Staphylococcus aureus-infected dynamic wound healing, Adv. Sci. 10 (2023) 2206585, https://doi.org/10.1002/advs.202206585.

[4] Y. Meng, L. Chen, Y. Chen, J. Shi, Z. Zhang, Y. Wang, F. Wu, X. Jiang, W. Yang, L. Zhang, C. Wang, X. Meng, Y. Wu, W. Bu, Reactive metal boride nanoparticles trap lipopolysaccharide and peptidoglycan for bacteria-infected wound healing, Nat. Commun. 13 (2022) 7353, https://doi.org/10.1038/s41467-022-35050-6.

[5] Z. Song, W. Yao, X. Zhang, Y. Dong, Z. Zhang, Y. Huang, W. Jing, L. Sun, Y. Han, F. Hu, Z. Yuan, B. Zhao, P. Wei, X. Zhang, Controlled growth of metal-organic frameworks on small intestinal submucosa for wound repair through combined antibacterial and angiogenic effects, Nano Today 54 (2024) 102060, https://doi.org/10.1016/j.nantod.2023.102060.

[6] T. Liu, M. Ma, A. Ali, Q. Liu, R. Bai, K. Zhang, Y. Guan, Y. Wang, J. Liu, H. Zhou, Self-assembled copper tannic acid nanoparticles: a powerful nano-bactericide by valence shift of copper, Nano Today 54 (2024) 102071, https://doi.org/10.1016/j.nantod.2023.102071.

[7] E.A. Kamoun, E.-R.S. Kenawy, X. Chen, A review on polymeric hydrogel membranes for wound dressing applications: PVA-based hydrogel dressings, J. Adv. Res. 8 (2017) 217–233, https://doi.org/10.1016/j.jare.2017.01.005.

[8] Q. Shi, X. Luo, Z. Huang, A.C. Midgley, B. Wang, R. Liu, D. Zhi, T. Wei, X. Zhou, M. Qiao, J. Zhang, D. Kong, K. Wang, Cobalt-mediated multi-functional dressings promote bacteria-infected wound healing, Acta Biomater. 86 (2019) 465–479, https://doi.org/10.1016/j.actbio.2018.12.048.

[9] Y. Yang, M. Li, G. Pan, J. Chen, B. Guo, Multiple stimuli-responsive nanozyme-based cryogels with controlled NO release as self-adaptive wound dressing for infected wound healing, Adv. Funct. Mater. 33 (2023) 2214089, https://doi.org/10.1002/adfm.202214089.

[10] Y. Zhao, B. Yi, J. Hu, D. Zhang, G. Li, Y. Lu, Q. Zhou, Double cross-linked biomimetic hyaluronic acid-based hydrogels with thermo-stimulated self-contraction and tissue adhesiveness for accelerating post-wound closure and wound healing, Adv. Funct. Mater. 33 (2023) 2300710, https://doi.org/10.1002/adfm.202300710.

[11] X. Liu, Y. Sun, J. Wang, Y. Kang, Z. Wang, W. Cao, J. Ye, C. Gao, A tough, antibacterial and antioxidant hydrogel dressing accelerates wound healing and suppresses hypertrophic scar formation in infected wounds, Bioact. Mater. 34 (2024) 269–281, https://doi.org/10.1016/j.bioactmat.2023.12.019.

[12] H. Wang, J. Li, X. Yu, G. Yan, X. Tang, Y. Sun, X. Zeng, L. Lin, Cellulose nanocrystalline hydrogel based on a choline chloride deep eutectic solvent as

[13] Z. Hu, D. Liu, M. Wang, C. Yu, Z. Han, M. Xu, W. Yue, G. Nie, β-Alanine enhancing the crosslink of chitosan/poly-(γ-glutamic acid) hydrogel for a potential alkaline-adapted wound dressing, Int. J. Biol. Macromol. 231 (2023) 123157, https://doi.org/10.1016/j.ijbiomac.2023.123157.

[14] C. Liu, J. Ling, L.-Y. Yang, X. Ouyang, N. Wang, Chitosan-based carbon nitride-polydopamine-silver composite dressing with antibacterial properties for wound healing, Carbohydr. Polym. 303 (2023) 120436, https://doi.org/10.1016/j.carbpol.2022.120436.

[15] M.D. Figueroa-Pizano, I. Vélez, F.J. Peñas, P. Zavala-Rivera, A.J. Rosas-Durazo, A. D. Maldonado-Arce, M.E. Martínez-Barbosa, Effect of freeze-thawing conditions for preparation of chitosan-poly (vinyl alcohol) hydrogels and drug release studies, Carbohydr. Polym. 195 (2018) 476–485, https://doi.org/10.1016/j.carbpol.2018.05.004.

[16] C. Luo, A. Guo, J. Li, Z. Tang, F. Luo, Janus hydrogel to mimic the structure and property of articular cartilage, ACS Appl. Mater. Interfaces 14 (2022) 35434–35443, https://doi.org/10.1021/acsami.2c09706.

[17] X. Zhang, Z. Yin, Y. Guo, H. Huang, J. Zhou, L. Wang, J. Bai, Z. Fan, A facile and large-scale synthesis of a PVA/chitosan/collagen hydrogel for wound healing, New J. Chem. 44 (2020) 20776–20784, https://doi.org/10.1039/D0NJ04016A.

[18] J. Deng, E.-Q. Zhu, G.-F. Xu, N. Naik, V. Murugadoss, M.-G. Ma, Z. Guo, Z.-J. Shi, Overview of renewable polysaccharide-based composites for biodegradable food packaging applications, Green Chem. 24 (2022) 480–492, https://doi.org/10.1039/D1GC03898B.

[19] A. Paiva, R. Craveiro, I. Aroso, M. Martins, R.L. Reis, A.R.C. Duarte, Natural deep eutectic solvents – solvents for the 21st century, ACS Sustainable Chem. Eng. 2 (2014) 1063–1071, https://doi.org/10.1021/sc500096j.

[20] M. Khajavian, V. Vatanpour, R. Castro-Muñoz, G. Boczkaj, Chitin and derivative chitosan-based structures — preparation strategies aided by deep eutectic solvents: a review, Carbohydr. Polym. 275 (2022) 118702, https://doi.org/10.1016/j.carbpol.2021.118702.

[21] W. Li, X. Zhao, T. Huang, Y. Ren, W. Gong, Y. Guo, J. Wang, Q. Tu, Preparation of sodium hyaluronate/dopamine/AgNPs hydrogel based on the natural eutetic solvent as an antibacterial wound dressing, Int. J. Biol. Macromol. 191 (2021) 60–70, https://doi.org/10.1016/j.ijbiomac.2021.09.056.

[22] X. Su, Y. Luo, Z. Tian, Z. Yuan, Y. Han, R. Dong, L. Xu, Y. Feng, X. Liu, J. Huang, Ctenophore-inspired hydrogels for efficient and repeatable underwater specific adhesion to biotic surfaces, Mater. Horiz. 7 (2020) 2651–2661, https://doi.org/10.1039/D0MH01344G.

[23] H. Xiong, Z. Wang, C. Wang, J. Yao, Transforming complexity to simplicity: protein-like nanotransformer for improving tumor drug delivery programmatically, Nano Lett. 20 (2020) 1781–1790, https://doi.org/10.1021/acs.nanolett.9b05008.

[24] X. Lin, L. Zhang, B. Duan, Polyphenol-mediated chitin self-assembly for constructing a fully naturally resourced hydrogel with high strength and toughness, Mater. Horiz. 8 (2021) 2503–2512, https://doi.org/10.1039/D1MH00878A.

[25] A. Shavandi, A.E.-D.A. Bekhit, P. Saeedi, Z. Izadifar, A.A. Bekhit, A. Khademhosseini, Polyphenol uses in biomaterials engineering, Biomaterials 167 (2018) 91–106, https://doi.org/10.1016/j.biomaterials.2018.03.018.

[26] D. Li, J. Li, S. Wang, Q. Wang, W. Teng, Dually crosslinked copper-poly(tannic acid) nanoparticles with microenvironment-responsiveness for infected wound treatment, Adv. Healthcare Mater. 12 (2023) 2203063, https://doi.org/10.1002/adhm.202203063.

[27] S. You, Y. Xiang, X. Qi, R. Mao, E. Cai, Y. Lan, H. Lu, J. Shen, H. Deng, Harnessing a biopolymer hydrogel reinforced by copper/tannic acid nanosheets for treating bacteria-infected diabetic wounds, Materials Today Advances 15 (2022) 100271, https://doi.org/10.1016/j.mtadv.2022.100271.

[28] S. Zong, H. Lv, C. Liu, L. Zhu, J. Duan, J. Jiang, Mussel inspired Cu-tannic autocatalytic strategy for rapid self-polymerization of conductive and adhesive hydrogel sensors with extreme environmental tolerance, Chem. Eng. J. 465 (2023) 142831, https://doi.org/10.1016/j.cej.2023.142831.

[29] D. Gan, W. Xing, L. Jiang, J. Fang, C. Zhao, F. Ren, L. Fang, K. Wang, X. Lu, Plant-inspired adhesive and tough hydrogel based on Ag-Lignin nanoparticles-triggered dynamic redox catechol chemistry, Nat. Commun. 10 (2019) 1487, https://doi.org/10.1038/s41467-019-09351-2.

[30] Q. Wang, X. Pan, C. Lin, X. Ma, S. Cao, Y. Ni, Ultrafast gelling using sulfonated lignin-Fe3+ chelates to produce dynamic crosslinked hydrogel/coating with charming stretchable, conductive, self-healing, and ultraviolet-blocking properties, Chem. Eng. J. 396 (2020) 125341, https://doi.org/10.1016/j.cej.2020.125341.

[31] J. Li, J. Li, J. Wei, X. Zhu, S. Qiu, H. Zhao, Copper tannic acid-coordinated metal–organic nanosheets for synergistic antimicrobial and antifouling coatings, ACS Appl. Mater. Interfaces 13 (2021) 10446–10456, https://doi.org/10.1021/acsami.0c22321.

[32] Y. Wang, Y. Zou, Y. Wu, T. Wei, K. Lu, L. Li, Y. Lin, Y. Wu, C. Huang, Y. Zhang, H. Chen, Q. Yu, Universal antifouling and photothermal antibacterial surfaces based on multifunctional metal–phenolic networks for prevention of biofilm formation, ACS Appl. Mater. Interfaces 13 (2021) 48403–48413, https://doi.org/10.1021/acsami.1c14979.

[33] S. Lin, Y. Cheng, H. Zhang, X. Wang, Y. Zhang, Y. Zhang, L. Miao, X. Zhao, H. Wei, Copper tannic acid coordination nanosheet: a potent nanozyme for scavenging ROS from cigarette smoke, Small 16 (2020) 1902123, https://doi.org/10.1002/smll.201902123.

[34] G. He, Y. Zhou, X. Chen, T. Ma, Y. Yin, Y. Chu, L. Fan, W. Cai, Preparation of poly (vinyl alcohol)/polydopamine/tannin acid composite hydrogels with dual

adhesive, antioxidant and antibacterial properties, Eur. Polym. J. 205 (2024) 112708, https://doi.org/10.1016/j.eurpolymj.2023.112708.

[35] F. Azadikhah, A.R. Karimi, Injectable photosensitizing supramolecular hydrogels: a robust physically cross-linked system based on polyvinyl alcohol/chitosan/tannic acid with self-healing and antioxidant properties, React. Funct. Polym. 173 (2022) 105212, https://doi.org/10.1016/j.reactfunctpolym.2022.105212.

[36] D. Xie, C. Hu, C. Jiang, J. Xia, L. Ye, Y. Jin, S. Jiang, Y. Ji, Z. Zhang, H. Song, Y. Zhu, P. Tang, Z. Hu, Y. Xiao, J. Dai, Z. Hu, Incorporating copper-based nanosheets into an injectable self-healing hydrogel enables superb repair of infected diabetic wound, Chem. Eng. J. 476 (2023) 146788, https://doi.org/10.1016/j.cej.2023.146788.

[37] C. Luo, Y. Zhao, X. Sun, F. Luo, Fabrication of antiseptic, conductive and robust polyvinyl alcohol/chitosan composite hydrogels, J. Polym. Res. 27 (2020) 269, https://doi.org/10.1007/s10965-020-02247-6.

[38] T. Huang, Y. Zhang, L. Zhao, Y. Ren, K. Wang, N. Zhang, X. Zhang, J. Wang, Q. Tu, Sodium hyaluronate hydrogel for wound healing and human health monitoring based on deep eutectic solvent, Int. J. Biol. Macromol. 257 (2024) 128801, https://doi.org/10.1016/j.ijbiomac.2023.128801.

[39] Q. Ding, C. Ding, X. Liu, Y. Zheng, Y. Zhao, S. Zhang, S. Sun, Z. Peng, W. Liu, Preparation of nanocomposite membranes loaded with taxifolin liposome and its mechanism of wound healing in diabetic mice, Int. J. Biol. Macromol. 241 (2023) 124537, https://doi.org/10.1016/j.ijbiomac.2023.124537.

[40] T. Liu, M. Ma, A. Ali, Q. Liu, R. Bai, K. Zhang, Y. Guan, Y. Wang, J. Liu, H. Zhou, Self-assembled copper tannic acid nanoparticles: a powerful nano-bactericide by valence shift of copper, Nano Today 54 (2024) 102071, https://doi.org/10.1016/j.nantod.2023.102071.

[41] K. Yang, X. Zhou, Z. Li, Z. Wang, Y. Luo, L. Deng, D. He, Ultrastretchable, self-healable, and tissue-adhesive hydrogel dressings involving nanoscale tannic acid/ferric ion complexes for combating bacterial infection and promoting wound healing, ACS Appl. Mater. Interfaces 14 (2022) 43010–43025, https://doi.org/10.1021/acsami.2c13283.

[42] Y. Wu, Y. Wang, L. Long, C. Hu, Q. Kong, Y. Wang, A spatiotemporal release platform based on pH/ROS stimuli-responsive hydrogel in wound repairing, J. Contr. Release 341 (2022) 147–165, https://doi.org/10.1016/j.jconrel.2021.11.027.

[43] N. Zhao, W. Yuan, Self-healing and shape-adaptive nanocomposite hydrogels with anti-inflammatory, antioxidant, antibacterial activities and hemostasis for real-time visual regeneration of diabetic wounds, Compos. B Eng. 262 (2023) 110819, https://doi.org/10.1016/j.compositesb.2023.110819.

[44] K. Chen, Z. Wu, Y. Liu, Y. Yuan, C. Liu, Injectable double-crosslinked adhesive hydrogels with high mechanical resilience and effective energy dissipation for joint wound treatment, Adv. Funct. Mater. 32 (2022) 2109687, https://doi.org/10.1002/adfm.202109687.

[45] Z. Liang, J. Luo, S. Liu, Y. Gu, Z. Cui, Y. Zhu, Z. Yu, X. Zhao, B. Guo, B. Song, Injectable, antibacterial, ROS scavenging and pro-angiogenic hydrogel adhesives promote chronic wound healing in diabetes via synergistic release of NMN and Mg2+, Chem. Eng. J. 475 (2023) 146092 https://doi.org/10.1016/j.cej.2023.146092.

[46] A. Ko, C. Liao, Hydrogel wound dressings for diabetic foot ulcer treatment: status-quo, challenges, and future perspectives, BMEMat 1 (2023) e12037, https://doi.org/10.1002/bmm2.12037.

[47] Z. Ahmadian, A. Correia, M. Hasany, P. Figueiredo, F. Dobakhti, M.R. Eskandari, S.H. Hosseini, R. Abiri, S. Khorshid, J. Hirvonen, H.A. Santos, M.-A. Shahbazi, A hydrogen-bonded extracellular matrix-mimicking bactericidal hydrogel with radical scavenging and hemostatic function for pH-responsive wound healing acceleration, Adv. Healthcare Mater. 10 (2021) 2001122, https://doi.org/10.1002/adhm.202001122.

[48] W. Feng, Z. Wang, Tailoring the swelling-shrinkable behavior of hydrogels for biomedical applications, Adv. Sci. 10 (2023) 2303326, https://doi.org/10.1002/advs.202303326.

[49] S. Abdolmaleki, A. Aliabadi, S. Khaksar, Unveiling the promising anticancer effect of copper-based compounds: a comprehensive review, J. Cancer Res. Clin. Oncol. 150 (2024) 213, https://doi.org/10.1007/s00432-024-05641-5.

[50] Y. Zhang, Y. Wang, L. Chen, J. Zheng, X. Fan, X. Xu, G. Zhou, N. Ullah, X. Feng, An injectable antibacterial chitosan-based cryogel with high absorbency and rapid shape recovery for noncompressible hemorrhage and wound healing, Biomaterials 285 (2022) 121546, https://doi.org/10.1016/j.biomaterials.2022.121546.

[51] L. Zheng, H. Hua, Z. Zhang, Y. Zhu, L. Wang, Y. Li, PVA/ChCl deep eutectic polymer blends for transparent strain sensors with antifreeze, flexible, and recyclable properties, ACS Appl. Mater. Interfaces 14 (2022) 49212–49223, https://doi.org/10.1021/acsami.2c15673.

[52] Y. Wang, Y. Wang, L. Yan, Deep eutectic solvent-induced microphase separation and entanglement of PVA chains for tough and reprocessable eutectogels for sensors, Langmuir 38 (2022) 12189–12197, https://doi.org/10.1021/acs.langmuir.2c01770.

[53] Y. Tian, F. Jiang, H. Xie, Z. Chi, C. Liu, Conductive Hyaluronic Acid/Deep Eutectic Solvent Composite Hydrogel as a Wound Dressing for Promoting Skin Burn Healing Under Electrical Stimulation, Advanced Healthcare Materials n/a (n.d.) 2304117. https://doi.org/10.1002/adhm.202304117.

[54] T. Lan, Y. Dong, J. Shi, X. Wang, Z. Xu, Y. Zhang, L. Jiang, W. Zhou, X. Sui, Advancing self-healing soy protein hydrogel with dynamic Schiff base and metal-ligand bonds for diabetic chronic wound recovery, Aggregate n/a (n.d.) e639. https://doi.org/10.1002/agt2.639.

[55] R. Zhou, W. Zhang, J. Huang, W. Peng, W. Wang, R. Bo, M. Liu, J. Li, A hydrogel dressing loaded with tea tree oil nanoemulsion accelerates *methicillin-resistant Staphylococcus aureus*-infected wound healing, Mater. Today Commun. 39 (2024) 109218, https://doi.org/10.1016/j.mtcomm.2024.109218.

[56] W. Feng, Z. Wang, Shear-thinning and self-healing chitosan-graphene oxide hydrogel for hemostasis and wound healing, Carbohydr. Polym. 294 (2022) 119824, https://doi.org/10.1016/j.carbpol.2022.119824.

[57] A. Kumar, D.K. Sah, K. Khanna, Y. Rai, A.K. Yadav, M.S. Ansari, A.N. Bhatt, A calcium and zinc composite alginate hydrogel for pre-hospital hemostasis and wound care, Carbohydr. Polym. 299 (2023) 120186, https://doi.org/10.1016/j.carbpol.2022.120186.

[58] Y. Li, R. Fu, Z. Duan, C. Zhu, D. Fan, Artificial nonenzymatic antioxidant MXene nanosheet-anchored injectable hydrogel as a mild photothermal-controlled oxygen release platform for diabetic wound healing, ACS Nano 16 (2022) 7486–7502, https://doi.org/10.1021/acsnano.1c10575.

[59] S. Lv, S. Zhang, J. Zuo, S. Liang, J. Yang, J. Wang, D. Wei, Progress in preparation and properties of chitosan-based hydrogels, Int. J. Biol. Macromol. 242 (2023) 124915, https://doi.org/10.1016/j.ijbiomac.2023.124915.

[60] X. Yu, C. Cheng, X. Peng, K. Zhang, X. Yu, A self-healing and injectable oxidized quaternized guar gum/carboxymethyl chitosan hydrogel with efficient hemostatic and antibacterial properties for wound dressing, Colloids Surf. B Biointerfaces 209 (2022) 112207, https://doi.org/10.1016/j.colsurfb.2021.112207.

[61] Y. Lu, X. Zhu, C. Hu, P. Li, M. Zhao, J. Lu, G. Xia, A fucoidan-gelatin wound dressing accelerates wound healing by enhancing antibacterial and anti-inflammatory activities, Int. J. Biol. Macromol. 223 (2022) 36–48, https://doi.org/10.1016/j.ijbiomac.2022.10.255.

[62] Q. Wu, R. Yang, W. Fan, L. Wang, J. Zhan, T. Cao, Q. Liu, X. Piao, Y. Zhong, W. Zhao, S. Zhang, J. Yu, S. Liang, T.M. Roberts, B. Wang, Z. Liu, Spermidine-functionalized injectable hydrogel reduces inflammation and enhances healing of acute and diabetic wounds in situ, Adv. Sci. 11 (2024) 2310162, https://doi.org/10.1002/advs.202310162.

[63] G. Wang, N. Yuan, J. Zhang, M. Qin, S. Dong, Y. Wang, Visible light cross-linking and bioactive peptides loaded integrated hydrogel with sequential release to accelerate wound healing complicated by bacterial infection, Nano Res. (2023), https://doi.org/10.1007/s12274-023-5958-6.

[64] Y. Yu, R. Tian, Y. Zhao, X. Qin, L. Hu, J.-J. Zou, Y.-W. Yang, J. Tian, Self-assembled corrole/chitosan photothermal nanoparticles for accelerating infected diabetic wound healing, Adv. Healthcare Mater. 12 (2023) 2201651, https://doi.org/10.1002/adhm.202201651.

[65] J. Qu, X. Zhao, Y. Liang, T. Zhang, P.X. Ma, B. Guo, Antibacterial adhesive injectable hydrogels with rapid self-healing, extensibility and compressibility as wound dressing for joints skin wound healing, Biomaterials 183 (2018) 185–199, https://doi.org/10.1016/j.biomaterials.2018.08.044.

[66] X. Liang, L. Ding, J. Ma, J. Li, L. Cao, H. Liu, M. Teng, Z. Li, Y. Peng, H. Chen, Y. Zheng, H. Cheng, G. Liu, Enhanced Mechanical Strength and Sustained Drug Release in Carrier-Free Silver-Coordinated Anthraquinone Natural Antibacterial Anti-Inflammatory Hydrogel for Infectious Wound Healing, Advanced Healthcare Materials n/a (n.d.) 2400841. https://doi.org/10.1002/adhm.202400841.

[67] A. Uberoi, A. McCready-Vangi, E.A. Grice, The wound microbiota: microbial mechanisms of impaired wound healing and infection, Nat. Rev. Microbiol. 22 (2024) 507–521, https://doi.org/10.1038/s41579-024-01035-z.

[68] M. Zhu, J. Ou, Y. Chen, Y. Tian, W. Song, X. Hu, X. Ju, S. Jiang, S. Huang, Z. Niu, Programming of macrophage polarization in different stages for accelerating wound healing, Chem. Eng. J. 491 (2024) 152131, https://doi.org/10.1016/j.cej.2024.152131.

[69] S. Guo, Y. Ren, R. Chang, Y. He, D. Zhang, F. Guan, M. Yao, Injectable self-healing adhesive chitosan hydrogel with antioxidative, antibacterial, and hemostatic activities for rapid hemostasis and skin wound healing, ACS Appl. Mater. Interfaces (2022), https://doi.org/10.1021/acsami.2c08870.

[70] S. Zhu, B. Zhao, M. Li, H. Wang, J. Zhu, Q. Li, H. Gao, Q. Feng, X. Cao, Microenvironment responsive nanocomposite hydrogel with NIR photothermal therapy, vascularization and anti-inflammation for diabetic infected wound healing, Bioact. Mater. 26 (2023) 306–320, https://doi.org/10.1016/j.bioactmat.2023.03.005.

[71] P. Martin, D.B. Gurevich, Macrophage regulation of angiogenesis in health and disease, Semin. Cell Dev. Biol. 119 (2021) 101–110, https://doi.org/10.1016/j.semcdb.2021.06.010.